

Check for updates

The Plant Journal (2024) doi: 10.1111/tpj.16933

Formate-tetrahydrofolate ligase: supplying the cytosolic one-carbon network in roots with one-carbon units originating from glycolate

Sompop Saeheng^{1,2,3,†}, Clayton Bailes^{1,†}, Han Bao⁴, Kelem Gashu^{4,5}, Matt Morency^{4,5}, Tana Arlynn¹, Andrei Smertenko¹, Berkley James Walker^{4,5}, and Sanja Roje^{1,*}

Received 4 May 2022; accepted 3 July 2024.

SUMMARY

The metabolism of tetrahydrofolate (H₄PteGlu_n)-bound one-carbon (C₁) units (C₁ metabolism) is multifaceted and required for plant growth, but it is unclear what of many possible synthesis pathways provide C₁ units in specific organelles and tissues. One possible source of C1 units is via formate-tetrahydrofolate ligase, which catalyzes the reversible ATP-driven production of 10-formyltetrahydrofolate (10-formyl-H₄. PteGlu_n) from formate and tetrahydrofolate (H₄PteGlu_n). Here, we report biochemical and functional characterization of the enzyme from Arabidopsis thaliana (AtFTHFL). We show that the recombinant AtFTHFL has lower K_m and k_{cat} values with pentaglutamyl tetrahydrofolate (H₄PteGlu₅) as compared to monoglutamyl tetrahydrofolate (H₄PteGlu₁), resulting in virtually identical catalytic efficiencies for the two substrates. Stable transformation of Arabidopsis plants with the EGFP-tagged AtFTHFL, followed with fluorescence microscopy, demonstrated cytosolic signal. Two independent T-DNA insertion lines with impaired AtFTHFL function had shorter roots compared to the wild type plants, demonstrating the importance of this enzyme for root growth. Overexpressing AtFTHFL led to the accumulation of H_4 PteGlu_n + 5,10-methylene- H_4 PteGlu_n and serine, accompanied with the depletion of formate and glycolate, in roots of the transgenic Arabidopsis plants. This metabolic adjustment supports the hypothesis that AtFTHFL feeds the cytosolic C₁ network in roots with C₁ units originating from glycolate, and that these units are then used mainly for biosynthesis of serine, and not as much for the biosynthesis of 5-methyl- H_4 PteGlu_n, methionine, and S-adenosylmethionine. This finding has implications for any future attempts to engineer one-carbon unit-requiring products through manipulation of the one-carbon metabolic network in non-photosynthetic organs.

Keywords: 10-formyltetrahydrofolate ligase, 10-formyltetrahydrofolate, one-carbon metabolism, *Arabidopsis thaliana*, folates, glycolate.

INTRODUCTION

The core metabolism of tetrahydrofolate ($H_4PteGlu_n$)-bound one-carbon (C_1) units (C_1 metabolism), essential to plants and other organisms, consists of reactions that add or remove C_1 units from $H_4PteGlu_n$, or change the oxidation state of the C_1 - $H_4PteGlu_n$ derivatives. The folate species including 10-formyl- $H_4PteGlu_n$, 5,10-methenyl- $H_4PteGlu_n$, 5,10-methylene- $H_4PteGlu_n$, and 5-methyl- $H_4PteGlu_n$ act as the donors of C_1

units in different oxidation states for reactions along multiple fundamental metabolic pathways, including the pathways that produce formyl-methionyl tRNA, glycine, methionine, pantothenate, purines, serine, and thymidylate, while 5-formyl-H₄PteGlu_n is an important regulatory molecule (Cossins, 1987; Hanson & Gregory III, 2011; Hanson & Roje, 2001). The metabolic sources for these C₁ units vary primarily based on the organelle and the tissues involved. The source

© 2024 The Author(s).

The Plant Journal published by Society for Experimental Biology and John Wiley & Sons Ltd.

¹Institute of Biological Chemistry, Washington State University, Pullman, Washington, USA,

²Center of Excellence for Biochemistry, Faculty of Science, Prince of Songkla University, Hat Yai 90110, Thailand,

³Plant Cell and Physiology for Sustainable Agriculture Research Unit, Faculty of Science, Prince of Songkla University, Hat Yai 90110, Thailand,

⁴Department of Energy-Michigan State University Plant Research Laboratory, Michigan State University, East Lansing, Michigan, USA, and

⁵Department of Plant Biology, Michigan State University, East Lansing, Michigan, USA

^{*}For correspondence (e-mail sanja@wsu.edu).

[†]These authors contributed equally to this work.

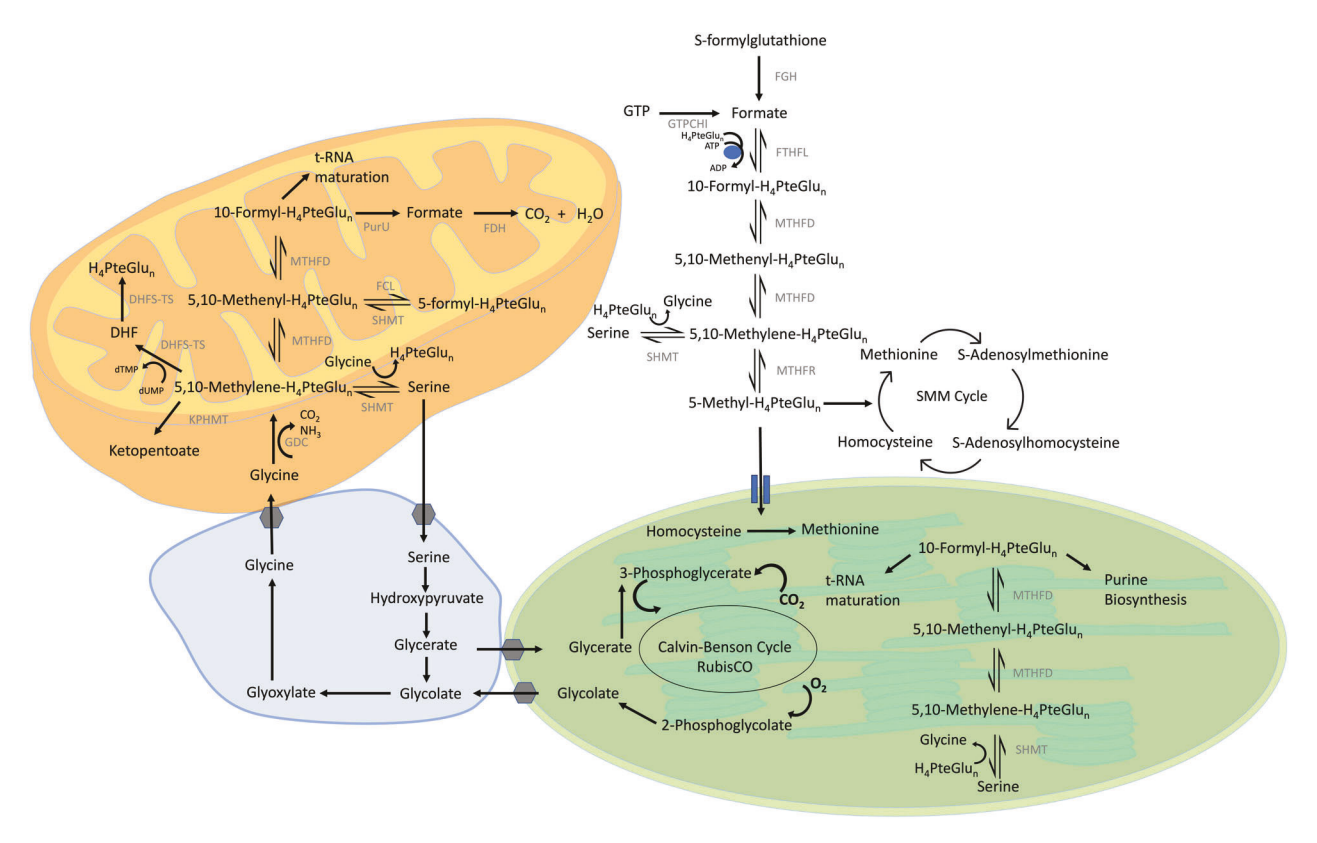


Figure 1. Subcellular compartmentation of the C₁ metabolic network and associated reactions in plants. ADP, adenosine diphosphate; ATP, adenosine triphosphate; DHF, dihydrofolate; DHFR-TS; dihydrofolate reductase-thymidylate synthase; dTMP, deoxythymidine monophosphate; dUMP, deoxyuridine monophosphate; FCL, 5-formyltetrahydrofolate cycloligase; FDH, formate dehydrogenase; FGH, S-formylglutathione hydrolase; FTHFL, formyltetrahydrofolate ligase; GDC, glycine decarboxylase complexes; GTP, guanosine triphosphate; GTPCHI, GTP cyclohydrolase I; H₄PteGlu_n, tetrahydrofolate; KPHMT, ketopantoate hydroxymethyltransferase; MTHFD, bifunctional methylenetetrahydrofolate dehydrogenase/methenyltetrahydrofolate cyclohydrolase; MTHFR, methylenetetrahydrofolate reductase; PurU, 10-formyltetrahydrofolate deformylase; SHMT, serine hydroxymethyltransferase.

metabolites for C₁ units in plants include serine, glycine, and formate. The supply of C₁ units from one or more source metabolites into the core C₁ metabolism is regulated by enzymes in the mitochondria, plastids, and the cytosol.

In mitochondria, glycine is thought to be the main C₁ donor metabolite. In a reaction catalyzed by the mitochondrial glycine decarboxylase, 5,10-methylene-H₄PteGlu_n is generated from glycine and H₄PteGlu_n, with the release of CO₂, and NH₃; the flux through this reaction is particularly high in photorespiring green tissues (Bauwe & Kolukisaoglu, 2003; Douce et al., 2001; Kisaki et al., 1971; Peterhansel et al., 2010). 5,10-methylene-H₄PteGlu_n can then be enzymatically oxidized to 5,10-methenyl-H₄PteGlu_n and further to 10-formyl-H₄PteGlu_n via the reversible reactions catalyzed by 5,10-methenyl-H₄PteGlu_n cyclohydrolase/5,10methylene-H₄PteGlu_n dehydrogenase (MTHFD) (Figure 1) (Groth et al., 2016; Kirk et al., 1995). 10-formyl-H₄PteGlu_n contributes its formyl moiety to maturation N-formylmethionyl-tRNA, which is essential to initiate translation (Dirk et al., 2001; Serero et al., 2001). 5,10methylene-H₄PteGlu_n is the C₁ unit donor in the formation of deoxythymidine monophosphate, which is required for DNA biosynthesis (Neuburger et al., 1996), and in the formation of ketopantoate, which is required for vitamin B5 biosynthesis (Smith et al., 2007). 5,10-methylene-H₄PteGlu_n is used to generate serine through the action of serine hydroxymethyltransferase, which catalyzes the reversible conversion of glycine and 5,10-methylene-H₄PteGlu_n to serine and H₄PteGlu_n (Douce et al., 2001). This serine is in leaves mostly processed through the photorespiratory pathway, although there is some evidence that substantial amounts are diverted into alternative metabolism pathways such as amino acid synthesis (Busch et al., 2018; Fu et al., 2022; Mouillon et al., 1999; Zimmermann et al., 2021).

In plastids, serine is most likely the sole C₁ donor because plastids lack enzymes that could utilize formate or glycine as the C₁ donors (Figure 1). In photosynthetic tissues, serine can be produced either through photorespiration, or through the phosphorylated serine biosynthesis pathway located in plastids (Ros et al., 2014). Heterotrophic tissues, which lack photorespiration, are thought to rely on the phosphorylated serine biosynthesis pathway (Ros et al., 2014) for serine production and this pathway shows a strong link to whole plant nitrogen metabolism

(Zimmermann et al., 2021). The plastidial SHMTs are thought to act in the direction opposite of the mitochondrial SHMTs in vivo, and to use serine and H₄PteGlu_n to produce glycine and 5,10-methylene-H₄PteGlu_n (Zhang et al., 2010). Then, 5,10-methylene-H₄PteGlu_n is enzymatically oxidized to 5,10-methenyl-H₄PteGlu_n and further to 10-formyl-H₄PteGlu_n by MTHFD, like in mitochondria (Hanson et al., 2000). In plastids, 10-formyl-H₄PteGlu_n is required for purine biosynthesis (Atkins et al., 1997; Liu & Ward, 2010; Rowe, 1984) and the production of Nformylmethionyl-tRNA (Staben & Rabinowitz, 1984).

Both serine and formate are the sources of C₁ units in the cytosol. Similar to what occurs in plastids, the cytosolic SHMTs employ serine as a C₁ donor to produce 5,10methylene-H₄PteGlu_n (Zhang et al., 2008). The cytosolic pool of serine can be obtained by importing serine produced in the plastids or mitochondria. In addition, serine can be generated from hydroxypyruvate by means of the alanine-hydroxypyruvate aminotransferase route (Niessen et al., 2007). Formate can be produced from a number of sources (Hanson & Roje, 2001; Hourton-Cabassa et al., 1998; Prabhu et al., 1996; Song et al., 2013; Wingler et al., 1999) and is a substrate for formate-tetrahydrofolate ligase (FTHFL), which catalyzes the reversible, ATP-driven formation of 10-formyl-H₄PteGlu_n from formate and H₄PteGlu_n (Himes & Rabinowitz, 1962; Rabinowitz & Pricer, 1956). The main precursors of formate in plant cells are thought to be glyoxylate and methanol. Glyoxylate is formed during photorespiration (Figure 1), the glyoxylate cycle, and purine degradation (Hourton-Cabassa et al., 1998; Kunze & Hartig, 2013). It is thought that the formate produced from non-enzymatic decarboxylation of glyoxylate during photorespiration in peroxisomes is channeled into cytosolic one-carbon metabolism via the FTHFL route (Hanson & Roie, 2001: Hourton-Cabassa et al., 1998: Prabhu et al., 1996; Wingler et al., 1999). The contributions to the formate pool from the glyoxylate cycle and purine degradation are at this point unclear. The main sources of methanol in plant cells are various de-methylation reactions (Dorokhov et al., 2018). The major contributor is thought to be the de-esterification of pectin into pectate and methanol, catalyzed by pectin methylesterases during cell wall remodeling (Pelloux et al., 2007). It is known that much of this methanol is released into air (Dorokhov et al., 2018); how much enters plant cells for internal processing is at this point unclear. Demethylation of histones, DNA, RNA, and proteins represents other notable sources of methanol in plant cells (Dorokhov et al., 2018). Methanol can be oxidized to formaldehyde by methanol oxidase (Hourton-Cabassa et al., 1998). Formaldehyde dehydrogenase then produces S-formylglutathione from formaldehyde and glutathione, while S-formylglutathione hydrolase catalyzes degradation of S-formylglutathione to formate and glutathione (Hourton-Cabassa et al., 1998; Kordic

et al., 2002). Formate is also produced in the cytosol during H₄PteGlu_n biosynthesis, in a reaction catalyzed by GTP cyclohydrolase I, which catalyzes conversion of GTP to formate and 7,8-dihydroneopterin triphosphate (Basset et al., 2002), and in plastids during riboflavin biosynthesis in a reaction catalyzed by GTP cyclohydrolase II, which catalyzes conversion of GTP to formate and 2,5-diamino-6ribosylamino-4(3H)-pyrimidinone 5'-phosphate (Roje, 2007). Given these numerous routes of formate formation depending on cellular compartment, it is critical to understand how formate and other C1 units are processed in vivo and in what tissue types these various pathways predominate, especially in root tissues that lack photorespiration-related biochemistries.

The role of plant FTHFLs in feeding C₁ metabolism and maintaining folate homeostasis is currently unclear. While other sources of C₁ units for one-carbon metabolism from serine or alvoine via serine hydroxymethyltransferases and glycine decarboxylase have been well studied (Bauwe & Kolukisaoglu, 2003; Moreno et al., 2005; Timm et al., 2012; Wei & Roje, 2011; Zhang et al., 2008, 2010), less is known about plant FTHFLs. The existence of FTHFL enzyme activity in higher plant species was first shown by purifying the enzyme from spinach leaves (Iwai et al., 1967b). The investigation of the enzyme purified from 7day-old pea seedlings provided evidence that the FTHFL enzyme binds to H_4 PteGlu_{n (n = 2-5)} more efficiently than to H₄PteGlu₁ in plants (Kirk et al., 1994). The FTHFL enzyme activity was detected predominantly in the cytosol, with only a small amount of it found in microsomes, mitochondria, and the nuclei in pea seedlings (Suzuki & Iwai, 1974). Another study showed an abundance of FTHFL activity in the cytosol in pea, but barely detected it in mitochondria with an immunoblotting technique (Chen et al., 1997). Based on the small amount of non-cytosolic activity found in these studies, the FTHFL reaction was proposed to exist in various subcellular compartments including mitochondria, chloroplasts, and the cytosol (Groth et al., 2016; Hanson et al., 2000; Peterhansel et al., 2010). In contrast, recent bioinformatic evidence suggests that FTHFL exclusively localizes to the cytosol in the examined algae and land plant species (Gorelova et al., 2019). A single copy of FTHFL is encoded in most of the algae and plant species. However, two copies of FTHFL have been detected in Glycine max, Linum usitatissimum, and Populus trichocarpa (Gorelova et al., 2019). The two homologs of FTHFL in G. max and P. trichocarpa are both predicted to be cytosolic as well. The available bioinformatic evidence therefore suggests that FTHFL functions in the cytosol in plants, and that the small amount of FTHFL activity that had been detected in other subcellular compartments previously was most likely due to a contamination from the cytosol.

Our study reports the biochemical characterization of a recombinant plant FTHFL and provides evidence that FTHFL is a cytosolic protein in Arabidopsis. The reduced root length compared to the wild type plants in the T-DNA insertion lines with impaired function of AtFTHFL demonstrates the importance of this enzyme in root growth and supports the hypothesis that FTHFL activity is important in C₁ metabolism in heterotrophic tissues, which lack photorespiratory-related metabolisms. The accumulation of H₄PteGlu_n + 5,10-methylene-H₄PteGlu_n and serine, along with the depletion of formate and glycolate, in roots of the transgenic Arabidopsis plants overexpressing AtFTHFL under control of the 35S promoter points to glycolate as an important source of C₁ units for roots. These findings fill a critical gap in knowledge of the C₁ metabolism in heterotrophic tissues by showing that FTHFL is an important player in roots, thus setting the stage for future studies determining how different source metabolites and enzymes ensure a sustained supply of C₁ units for the various essential metabolic processes in these tissues.

RESULTS

Catalytic properties of the recombinant AtFTHFL

The recombinant AtFTHFL enzyme was overexpressed in Escherichia coli and purified as described in Methods and was used to determine the steady-state kinetic parameters including the $K_{\rm m}$, $k_{\rm cat}$, and $V_{\rm max}$ values for ATP, formate, monoglutamyl tetrahydrofolate (H₄PteGlu₁), and pentaglutamyl tetrahydrofolate (H4PteGlu5), by assaying across a range of substrate concentrations (Figure S2; Table 1). All correlations between the substrate concentrations and the specific activity of the enzyme fit into the model of Michaelis-Menten kinetics. Comparison of the enzyme activity with H₄PteGlu₁ and H₄PteGlu₅ at different substrate concentrations showed that the $K_{\rm m}$ and $k_{\rm cat}$ values for H₄PteGlu_n, ATP, and formate decreased when the number of glutamates in the tail was increased from 1 to 5

Table 1 Apparent kinetic parameters of the recombinant AtFTHFL

Substrate	K _m (mM)	$k_{\rm cat}~({ m sec}^{-1})$	$k_{\rm cat}/K_{\rm m}~({\rm sec}^{-1}~{\rm M}^{-1})$
H ₄ PteGlu ₁ H ₄ PteGlu ₅ ATP ATP ₅ Formate Formate ₅	$\begin{array}{c} 0.76 \pm 0.07 \\ 0.09 \pm 0.009 \\ 2.51 \pm 0.4 \\ 0.22 \pm 0.02 \\ 2.18 \pm 0.2 \\ 0.22 \pm 0.005 \end{array}$	8.54 ± 0.75 1.29 ± 0.05 8.92 ± 0.15 1.28 ± 0.015 9.91 ± 0.24 1.19 ± 0.045	$\begin{array}{c} 1.11 \pm 0.01'10^4 \\ 1.33 \pm 0.08'10^4 \\ 0.37 \pm 0.05'10^4 \\ 0.53 \pm 0.04'10^4 \\ 0.41 \pm 0.03'10^4 \\ 0.58 \pm 0.04'10^4 \end{array}$

Kinetic parameters are best fits to the Michaelis-Menten model (SigmaPlot 14.5). The subscript 5 in the substrate name indicates that H₄PteGlu₁ was replaced with H₄PteGlu₅ in the enzyme assay. Data are the average \pm standard error of three independent determinations done in triplicate.

(Figure S2: Table 1). However, there was no detectible change in the catalytic efficiency (k_{cat}/K_m) for any of the substrates when H₄PteGlu₅ replaced H₄PteGlu₁ in the assays. Thus, it appears that the recombinant AtFTHFL uses H₄PteGlu₁ as efficiently as H₄PteGlu₅ in vitro.

AtFTHFL localizes to the cytosol

To investigate subcellular localization, AtFTHFL fused with either N- or C-terminal EGFP tag was stably expressed in Col-0 Arabidopsis plants under the control of the 35S promoter. Two-week-old transgenic plants were observed using laser scanning confocal microscopy. The EGFP signal of either the N- or C-terminal fusion AtFTHFL was detected only in the cytosol (Figure 2), supporting the bioinformatic prediction.

GUS reporter gene analysis shows strongest expression in cotyledons, root tips, and the vasculature

To understand the function of AtFTHFL in plant growth and development, the spatial and temporal expression pattern of AtFTHFL was determined with the β-glucuronidase (GUS) reporter gene fused to a 1.5-kb DNA fragment containing the AtFTHFL promoter in the binary vector pKGWFS7. Three independent transgenic lines were examined with GUS staining at the 3-day-old, 7-day-old, 11-dayold, and 15-day-old seedling stage.

At the 3-day-old seedling stage, the GUS activity was predominantly detected in cotyledons, columella and lateral root cap cells, and root vasculature (Figure 3a,d). At the later stages of development, the GUS activity illustrated AtFTHFL expression not only at the tip of the primary root but also at the tips of all lateral roots. The activity was also found in the vasculature in younger leaves (Figure 3b,c). The expression pattern of AtFTHFL in specific tissues during plant development therefore suggests that this enzyme plays predominantly a role in root

Generation of the AtFTHFL T-DNA insertion and 35S-driven overexpression lines

To find out how disruption of AtFTHFL activity affects plants in vivo, two independent T-DNA insertion lines (line A; Salk_054151 and line C; Salk_067510; Figure S3) were analyzed for AtFTHFL gene expression and enzyme activity (Figure 4). Both T-DNA insertion events led to highly reduced AtFTHFL gene expression in rosettes (Figure 4a) and roots (Figure 4c). Enzyme assays demonstrated only trace FTHFL activity in the two T-DNA insertion lines in comparison to wild type plants in both rosettes (Figure 4b) and roots (Figure 4d). Additionally, shoot activity was ~6-fold lower in shoot tissues of wild type as compared to root tissues as expressed on a protein basis. Therefore, both T-DNA insertion lines are strong knockdown alleles.

FTHFL is important for root growth 5

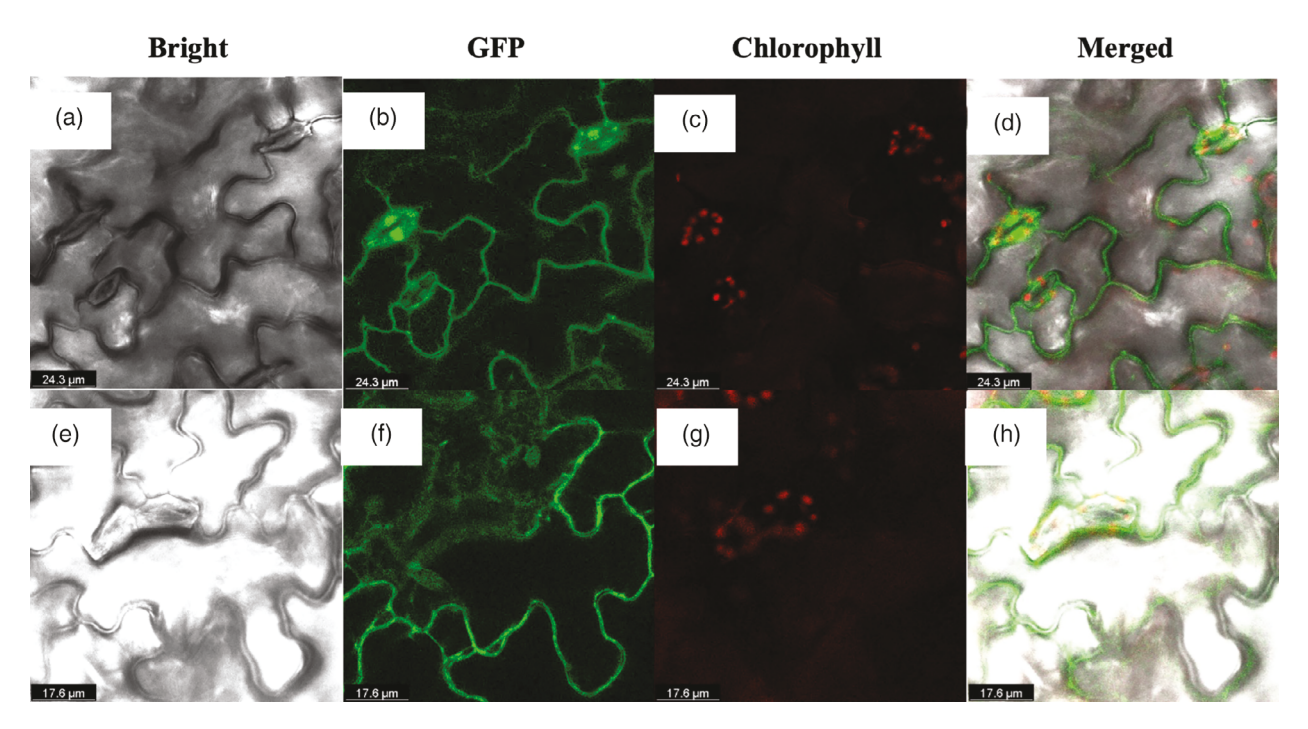


Figure 2. Confocal microscopy images of the Arabidopsis leaf epidermis from the transgenic plants expressing the coding sequence of AtFTHFL fused to the N-terminal (a–d) or C-terminal (e–h) EGFP.

(a, e) Bright-field; (b, f) EGFP; (c, g) chloroplast autofluorescence; and (d, h) the merged image.

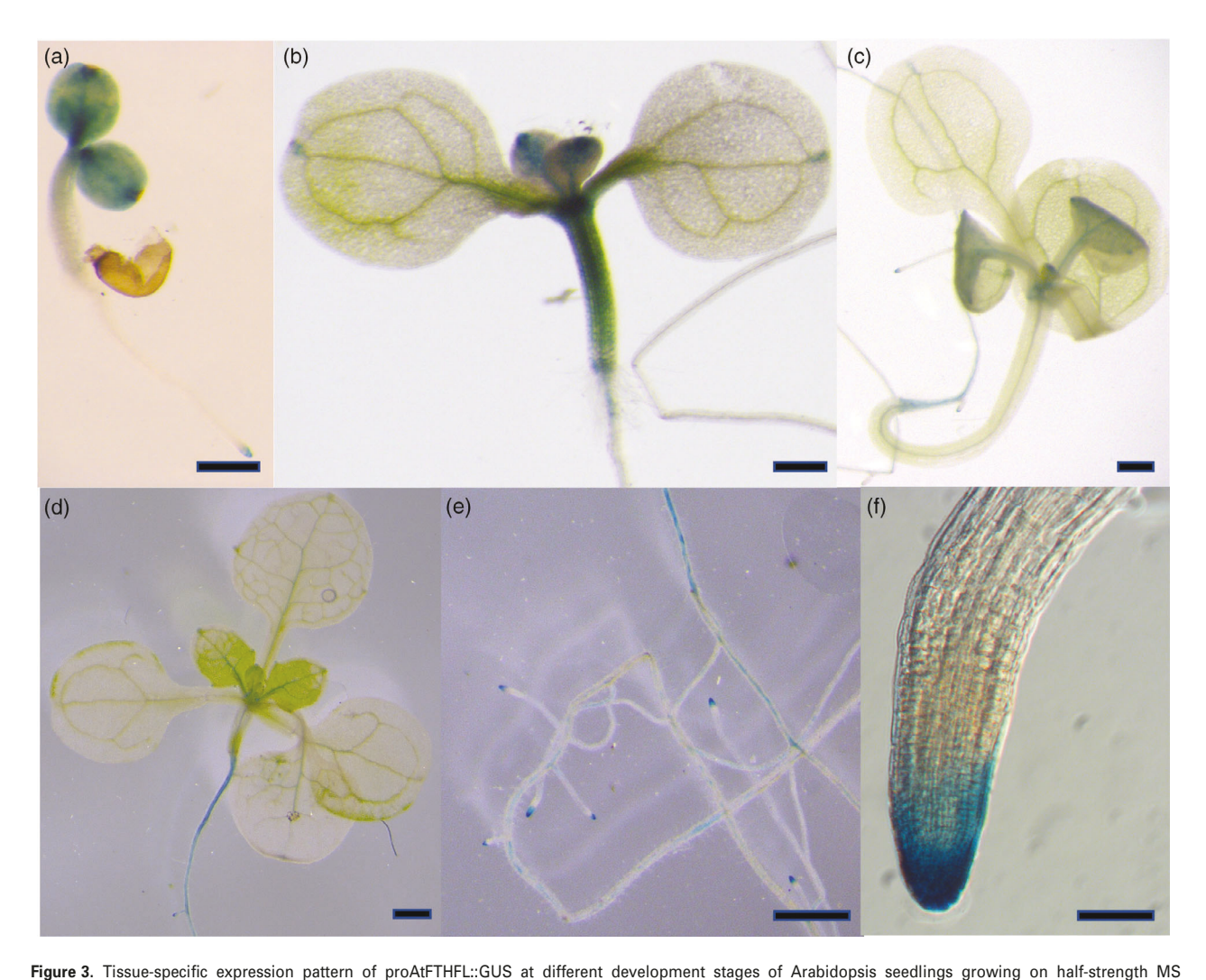
To resolve how increased AtFTHFL activity affects plants, 16 transgenic lines with a constitutively expressed AtFTHFL coding sequence (35S::AtFTHFL) were generated and screened. Three independent T₃ homozygous lines (denoted with OVE12, OVE16, and OVE21), which showed the highest levels of AtFTHFL expression, were selected for further analyses.

Both gene expression and AtFTHFL enzyme activity were investigated to verify overexpression in the T₃ homozygous lines. Compared with the wild type plants, the three independent overexpression lines (OVE12, OVE16, and OVE21) displayed 12- to 23-fold higher transcript accumulation in rosette tissues (Figure 4e), and 20-45 greater transcript accumulation in root tissues (Figure 4g). Next, an enzyme assay was conducted to examine whether the increase in transcript accumulation in the AtFTHFL overexpression lines directly translated to the higher amount of active AtFTHFL enzyme. The 8- to 12-fold higher enzyme activity was detected in the rosette tissues (Figure 4f) and 17- to 30-fold higher enzyme activity was found in root tissues (Figure 4h) of the overexpressors as compared to the wild type plants, consistent with the observed increase in the AtFTHFL transcript accumulation. Moreover, the AtFTHFL enzyme activity in wild type seedlings was nearly 6-fold higher in the root tissues relative to the rosette tissues (Figure 4b,d), which is consistent with the observed AtFTHFL promoter activity.

Growth parameters for the aerial parts of the T-DNA insertion and overexpression lines under standard growth conditions are unchanged, but the T-DNA insertion mutants have shorter roots compared to the wild type plants

To assess the potential role of AtFTHFL in plant growth and development, the T-DNA insertion lines (line A; Salk_054151 and line C; Salk_067510), the overexpressor lines (OVE12, OVE16, and OVE21), and the wild type plants were grown in a controlled environment growth chamber under standard conditions with a 16/8-h light/dark photoperiod. Specific growth parameters, including fresh weight, dry weight, height, and flowering time were monitored and recorded. There were no significant differences in fresh weight, dry weight, height, or flowering time in either the knockdown or the overexpression mutants when compared to the wild type plants (Figure S4).

The high activity of the *AtFTHFL* promoter in columella and lateral root cap cells suggests the importance of AtFTHFL for root growth. The primary root lengths of both T-DNA mutant lines A and C were statistically shorter in comparison with the Col-0 wild type plants (P < 0.01 for both) after 7 days of growth under short-day conditions (Figure 5). None of the overexpression lines showed significantly different root lengths compared to the wild type control plants. Lateral root density of these lines was also



medium: (a) 3 days after germination; (b) 7 days after germination; (c) 11 days after germination and (d–f) 15 days after germination.

Bars = 0.5 mm in (a), (b) and (e); 2 mm in (c), (d); 50 µm in (f). GUS staining is in lateral root cap at all developmental stages (a, c, e, f), in root vasculature (c–e) in cotyledons (a, b); but not detectable in leaves (b–d).

evaluated; none of the transgenics showed significant differences from the wild type plants.

To determine if the short root phenotype observed in knockdown lines A and C was a result of a smaller apical root meristem, the meristem lengths of mutant lines A and C were compared to that of wild type plants. Neither knockdown line showed a significant difference compared to the wild type (Figure S5).

To confirm that the short root phenotype in the T-DNA insertion lines was due to the reduction in the AtFTHFL gene expression, the T-DNA mutant line C, which has the more severe phenotype of the two lines we

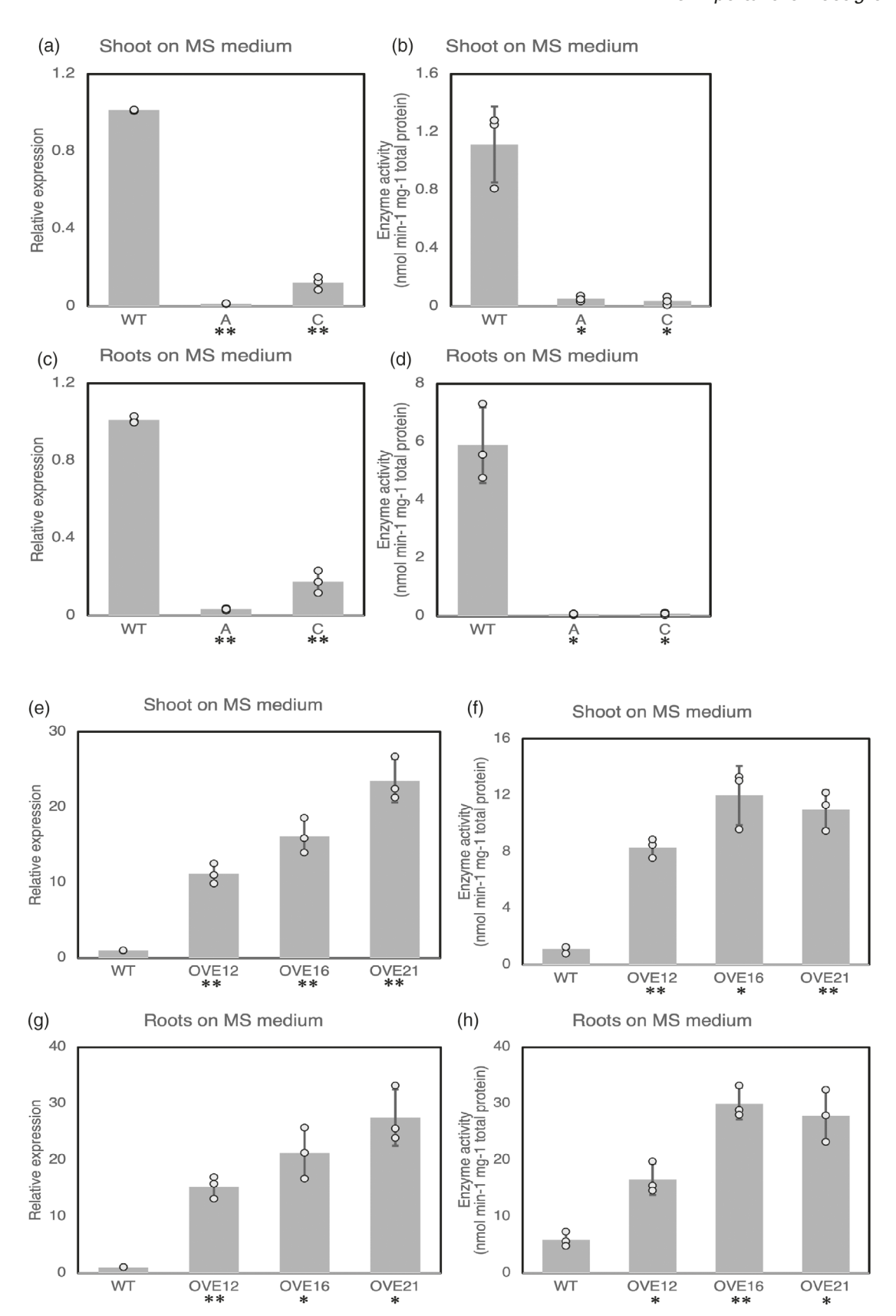
analyzed, was crossed with the overexpressor line OVE21. This cross fully complemented the short root phenotype, demonstrating that the reduction in the *AtFTHFL* gene expression was indeed responsible for the shorter root length in the T-DNA insertion lines (Figure S6).

Formate and folate pool size measurements are consistent with the FTHFL reaction operating in the direction of 10-formyl-H₄PteGlu_n formation *in vivo*

The enzyme assays conducted with the purified recombinant AtFTHFL and with the *Arabidopsis* extracts obtained from leaves and roots show that the AtFTHFL enzyme

Wild-type Columbia (WT) was used as a control. The data are an average of three triplicated experiments; error bars depict standard deviation. Asterisk indicates significant difference compared to the wild type (*P < 0.05; **P < 0.01).

Figure 4. AtFTHFL gene expression and enzyme activity levels in the AtFTHFL T-DNA insertion (A, Salk_054151 and C, Salk_067510) (a-d) and overexpression (OVE12, OVE16 and OVE21) (e-h) lines.



© 2024 The Author(s). The Plant Journal published by Society for Experimental Biology and John Wiley & Sons Ltd., The Plant Journal, (2024), doi: 10.1111/tpj.16933

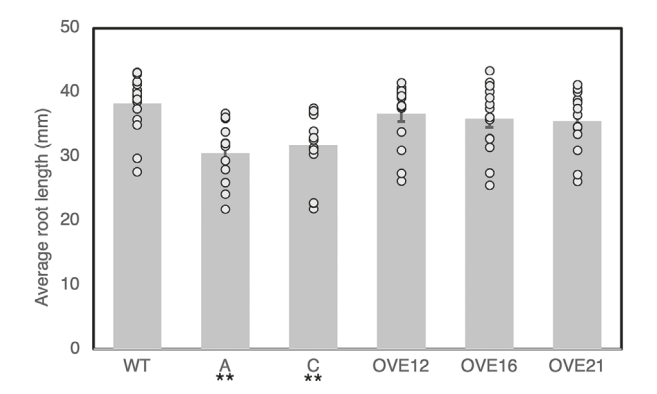


Figure 5. Quantitative analysis of the primary root lengths of 7-day-old seedlings was conducted on the two T-DNA insertion lines (A and C), three overexpressor lines (OVE12, OVE16 and OVE21), and the wild type (WT) plants.

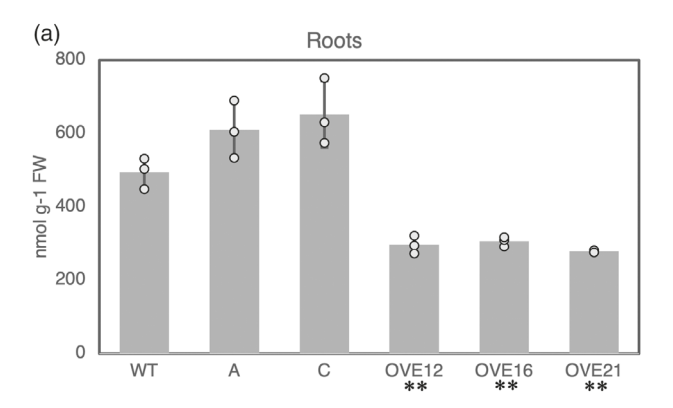
Error bars represent standard error from 30 plants grown in pairs (15 plates). Asterisk indicates significant difference compared to the wild type (*P < 0.05; **P < 0.01).

catalyzes the anticipated reaction in vitro. The question that remains is whether the reaction in vivo proceeds in the direction of production of 10-formyl-H₄PteGlu_n from formate and tetrahydrofolate (H₄PteGlu_n), or in the reverse direction. If AtFTHFL consumes formate as a substrate to generate 10-formyl-H₄PteGlu_n, then compared to the wild type plants, we expect to detect elevated formate pool size in the knockdown mutants and reduced formate pool size in the overexpressor mutants. A significant decrease in the formate pool size was observed in roots in all three overexpression lines compared to the wild type plants (P < 0.01) (Figure 6a). This result is consistent with the greater amount of active AtFTHFL enzyme leading to a higher rate of formate consumption, resulting in the depletion of the cellular formate pool in the AtFTHFL overexpression lines.

In leaves, the formate content did not differ in the AtFTHFL overexpressors or knockdowns when compared to the wild type plants (Figure 6b). One possible explanation is that formate-forming reactions replenish the formate pool more effectively in photosynthetic tissues than in non-photosynthetic tissues of the AtFTHFL overexpressors. Since photorespiration is thought to be the main source of formate in photosynthetic tissues, we measured formate contents in leaves of plants grown in high CO₂, which are expected to produce less formate through photorespiration (Figure 7). No difference in formate pool size was found in the AtFTHFL overexpressors or knockdowns when compared to the wild type plants, suggesting that processing of photorespiratory formate in leaves is not a major role of AtFTHFL.

We did not detect any difference in formate pool size in root or leaf tissues between the knockdowns and the wild type plants (Figure 6), suggesting the presence of alternative routes for formate processing that carry enough flux to maintain steady-state formate levels and compensate for the reduction in the FTHFL activity. This formate processing was not dependent on photorespiration in leaf tissues since when photorespiration was suppressed by growing plants under elevated CO₂ (2000 PPM), formate, folates, and amino acids remained similar across all genotypes (Figures 7, 9, and 11).

To look for another line of evidence supporting our hypothesis that AtFTHFL operates in the direction of 10-formyl-H₄PteGlu_n formation *in vivo*, we measured the steady-state levels of the C₁-folate species in roots and leaves of the transgenic and wild type plants. If our hypothesis is correct, we then expect that 10-formyl-H₄PteGlu_n or the downstream metabolites on the one-carbon pathway; 5,10-methenyl-H₄PteGlu_n, 5,10-methylene-H₄PteGlu_n and 5-methyl-H₄PteGlu_n, will be reduced in the knockdowns and increased in the overexpressors. As expected, there was a



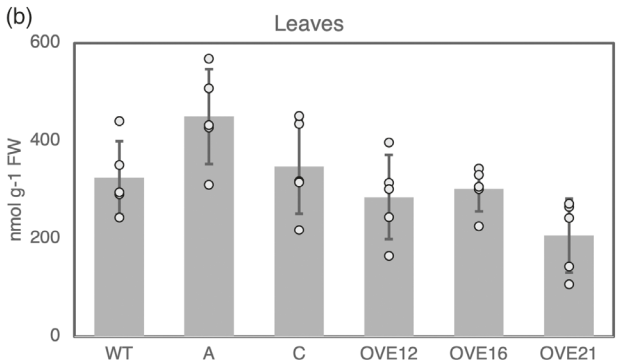


Figure 6. Formate levels in roots (a) and leaves (b) of the two T-DNA insertion lines (A and C), the three overexpressor lines (OVE12, OVE16 and OVE21), and the wild type (WT) plants.

Formate was measured using HPLC and presented on an absolute molar basis (nmol g^{-1} FW). The data are an average of three to five experiments; error bars depict standard deviation. Asterisk indicates significant difference compared to the wild type (*P < 0.05; **P < 0.01).



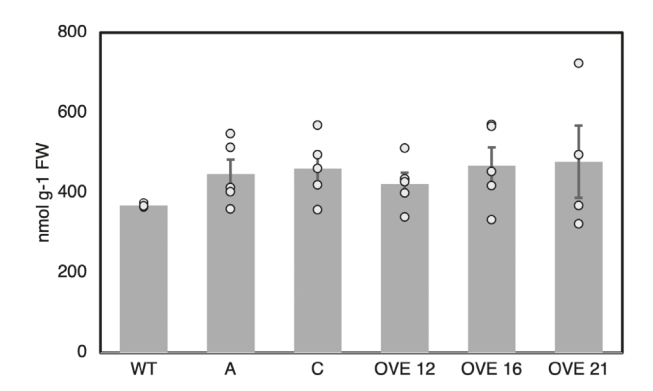


Figure 7. Formate levels in leaves of plants grown under elevated CO₂ of the two T-DNA insertion lines (A and C), the three overexpressor lines (OVE12, OVE16 and OVE21), and the wild type (WT) plants.

Formate was measured using HPLC and presented on an absolute molar basis (nmol g^{-1} FW). The data are an average of three to five experiments; error bars depict standard error. Asterisk indicates significant difference compared to the wild type (*P < 0.05; **P < 0.01).

significant increase in the $H_4PteGlu_n + 5,10$ -methylene- H_4 -Pte Glu_n contents in the roots of the three independent over-expression lines; OVE12 (P < 0.05), OVE16 (P < 0.05) and OVE21 (P < 0.01) when compared to the wild type plants (Figure 8a). Moreover, the 10-formyl- $H_4PteGlu_n + 5,10$ -methenyl- $H_4PteGlu_n$ level was significantly reduced in the knockdown line A (P < 0.01) (Figure 8a). The 5-methyl- H_4 -Pte Glu_n and total folate levels did not change in any transgenic lines relative to the wild type controls, suggesting that the change in AtFTHFL activity causes re-balancing of the C_1 -folate species without affecting the *de novo* folate biosynthesis in *Arabidopsis* roots (Figure 8).

Unlike in roots, we did not detect any differences compared to the wild type plants in the contents of the individual folate species and total folates in leaves of the knockdown or overexpressor plants grown under ambient conditions (Figure 8). Under elevated CO_2 conditions, the knockout line C showed a significant decrease in 5-methyl-H₄PteGlu_n compared to wild type (P=0.04). However, none of the other transgenics showed differences in any folate species compared to the wild type plants (Figure 9).

Amino acid and S-adenosylmethionine pool size measurements are consistent with increased flux into serine and not into 5-methyl- H_4 PteGlu_n in the roots of the overexpressors

We hypothesized that the elevated level of $H_4PteGlu_n + 5,10$ -methylene- $H_4PteGlu_n$ we detected in the overexpression lines is due to the accumulation of 5,10-methylene- H_4 -Pte Glu_n rather than that of $H_4PteGlu_n$, resulting from an increased influx of one-carbon units from formate into the cytosolic C_1 network. A method for distinguishing between $H_4PteGlu_n$ and 5,10-methylene- $H_4PteGlu_n$ in plant tissues is currently not available. Since 5,10-methylene- $H_4PteGlu_n$ is required for conversion of glycine to serine in the cytosol,

we hypothesized that the glycine and serine metabolic pools would change in the transgenics along with the pool of 5,10-methylene- H_4 PteGlu $_n$.

Significantly elevated serine levels in roots of the three independent overexpression lines, OVE12 (P < 0.05) OVE16 (P < 0.05) and OVE21 (P < 0.01) compared to the wild type plants (Figure 10), support our hypothesis that the elevated level of H_4 PteGlu_n + 5,10-methylene- H_{4-} PteGlu_n in the overexpressors is due to the accumulation of 5,10-methylene-H₄PteGlu_n rather than that of H₄PteGlu_n. Roots of the knockdown mutants showed no significant differences in glycine or serine contents compared to the wild type plants (Figure 10). This is consistent with the above measurements showing elevated formate and folate pools in the roots of overexpressors only, and no changes in the roots of the knockdown mutants. No difference in glycine and serine contents in leaves of the transgenic plants as compared to the wild type is consistent with unchanged formate and folate levels in these plants (Figures 6 and 8). Similarly, no differences in glycine or serine were observed in the leaves of transgenic plants grown under elevated CO₂ (Figure 11). Note that in these experiments, glycine, serine, and glycolic acid were measured using gas chromatography-mass spectrometry and are presented in relative abundances normalized to the ribitol peak and not absolute values. This results in metabolite values that are comparable on a relative basis between the same metabolite and different genotypes, but not between different metabolites or between separate experimental runs due to differences in instrument sensitivity and ion suppression, which change over time. Since methionine and AdoMet were measured using HPLC with authentic samples, they are presented here and elsewhere in molar concentrations per g fresh weight.

Under our standard procedure for collecting root tissue, the roots are grown vertically on agarose plates, which exposes them to light. To ensure that light exposure did not affect root metabolites, an additional set of roots were grown on plates where the roots were shielded from light. These plants were analyzed for serine and glycine (Figure S7). Like for roots grown in light, all three overexpression lines showed significantly elevated tissue contents of serine compared to wild type (P < 0.05 for each). Only one of the overexpression lines (OVE12) showed slightly elevated glycine compared to wild type. Neither knockdown line showed significant differences in serine or glycine compared to wild type. These results are therefore consistent with the findings observed in the unshielded roots.

The results presented above support the hypothesis that the extra C_1 units that enter the cytosolic one-carbon pool through AtFTHFL in the roots of overexpressor plants are used mostly for the biosynthesis of serine from glycine, and not so much for the biosynthesis of 5-methyl- H_4 . PteGlu_n and its downstream metabolites methionine and

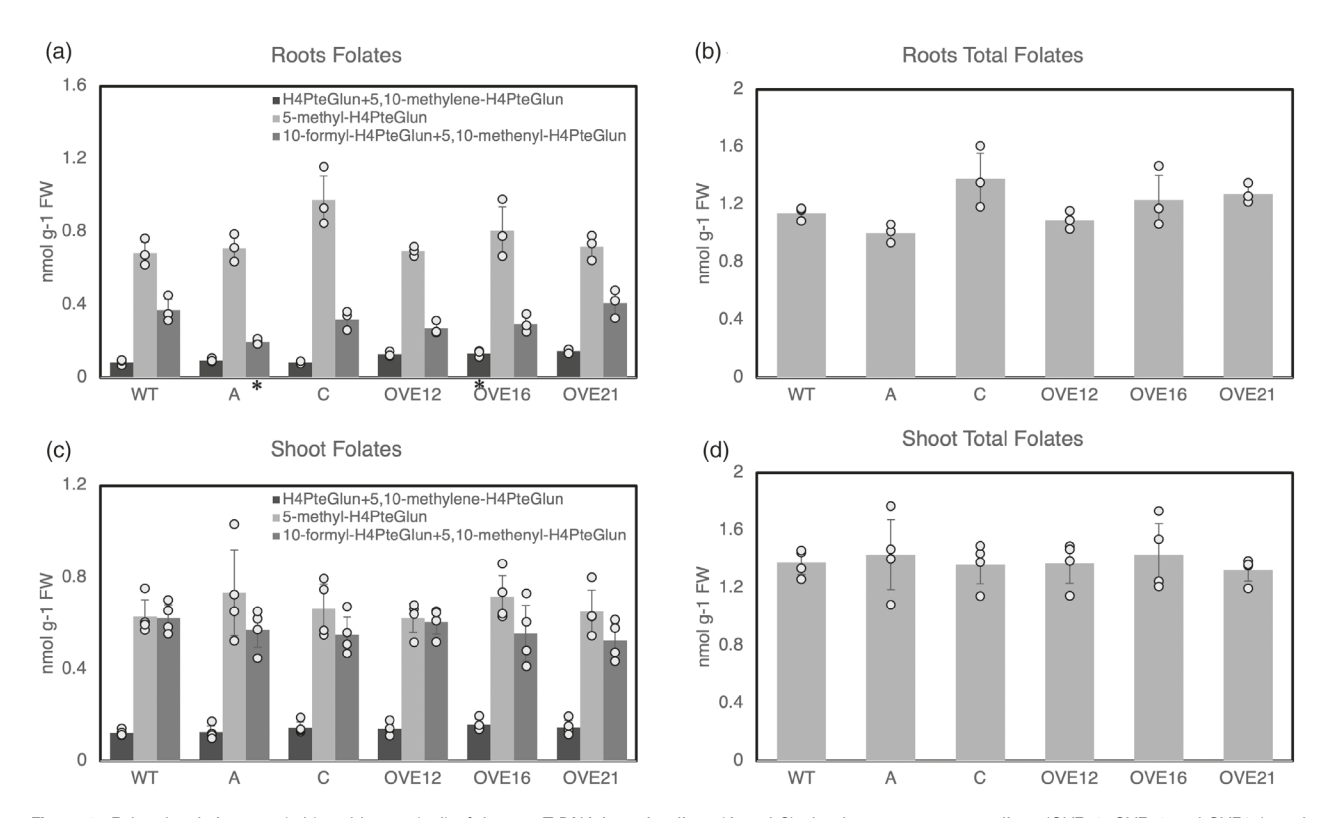


Figure 8. Folate levels in roots (a,b) and leaves (c,d) of the two T-DNA insertion lines (A and C), the three overexpressor lines (OVE12, OVE16 and OVE21), and the wild type (WT) plants.

Folates were measured using HPLC and presented on an absolute molar basis (nmol g⁻¹ FW). The data are an average of three to five experiments; error bars depict standard deviation. Asterisk indicates significant difference compared to the wild type (*P < 0.05; **P < 0.01).

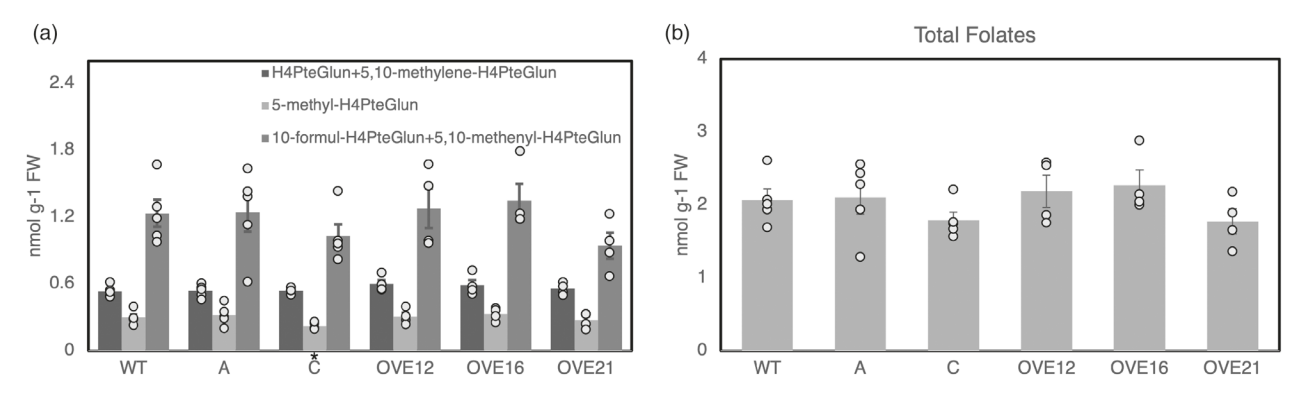


Figure 9. Individual (a) and total (b) folate levels in leaves of plants grown under elevated CO2 of the two T-DNA insertion lines (A and C), the three overexpressor lines (OVE12, OVE16 and OVE21), and the wild type (WT) plants. Folates were measured using HPLC and presented on an absolute molar basis (nmol g⁻¹ FW). The data are an average of three to five experiments; error bars depict standard error. Asterisk indicates significant difference compared to the wild type (*P < 0.05; **P < 0.01).

S-adenosylmethionine. To find another line of evidence supporting this hypothesis, we measured the pool sizes of methionine and S-adenosylmethionine in the transgenic and wild type plants. In support of our hypothesis, we found no change in the pool sizes of methionine and Sadenosylmethionine in any of the knockdown and overexpressor lines compared to the wild type plants in roots and rosettes (Figure 10). Similarly, no changes in methionine were found between the transgenic lines and wild type in the leaves of plants grown under elevated CO₂ (Figure 11).

Glycolate pool size measurements support increased use for serine biosynthesis in roots of the overexpressor

Others (Schmitz et al., 2020) have previously found an abundance of glycolate in heterotrophic plant tissues, and have hypothesized that this glycolate is used mainly as a source of the C_1 units for serine biosynthesis. Thus, to find out if the extra C_1 units needed for the increased serine biosynthesis in roots of the overexpressor plants may be coming from glycolate, we measured the pool sizes of this metabolite. Supporting the proposed hypothesis, we found a statistically significant decrease in glycolate in roots of the two overexpressors: OVE16 (P < 0.01) and OVE21 (P < 0.01) with the highest level of FTHFL activity (Figure 10).

No change in CO₂ assimilation in any of the AtFTHFL transgenic lines

To reveal if changes in the AtFTHFL activity in leaves may have caused changed in formate processing via the mitochondrial formate dehydrogenase, which converts formate to CO₂, we measured net CO₂ assimilation from the leaves of the AtFTHFL knockdown and overexpression plants in comparison to the wild type plants. We found no difference in rates of net CO₂ assimilation, which is consistent with no changes in the CO₂ release from processes like formate dehydrogenase in any of the AtFTHFL mutants relative to the wild type plants (Figure S8), suggesting no statistically significant change in formate processing *via* this route in leaves of any of the transgenic lines compared to the wild type plants.

DISCUSSION

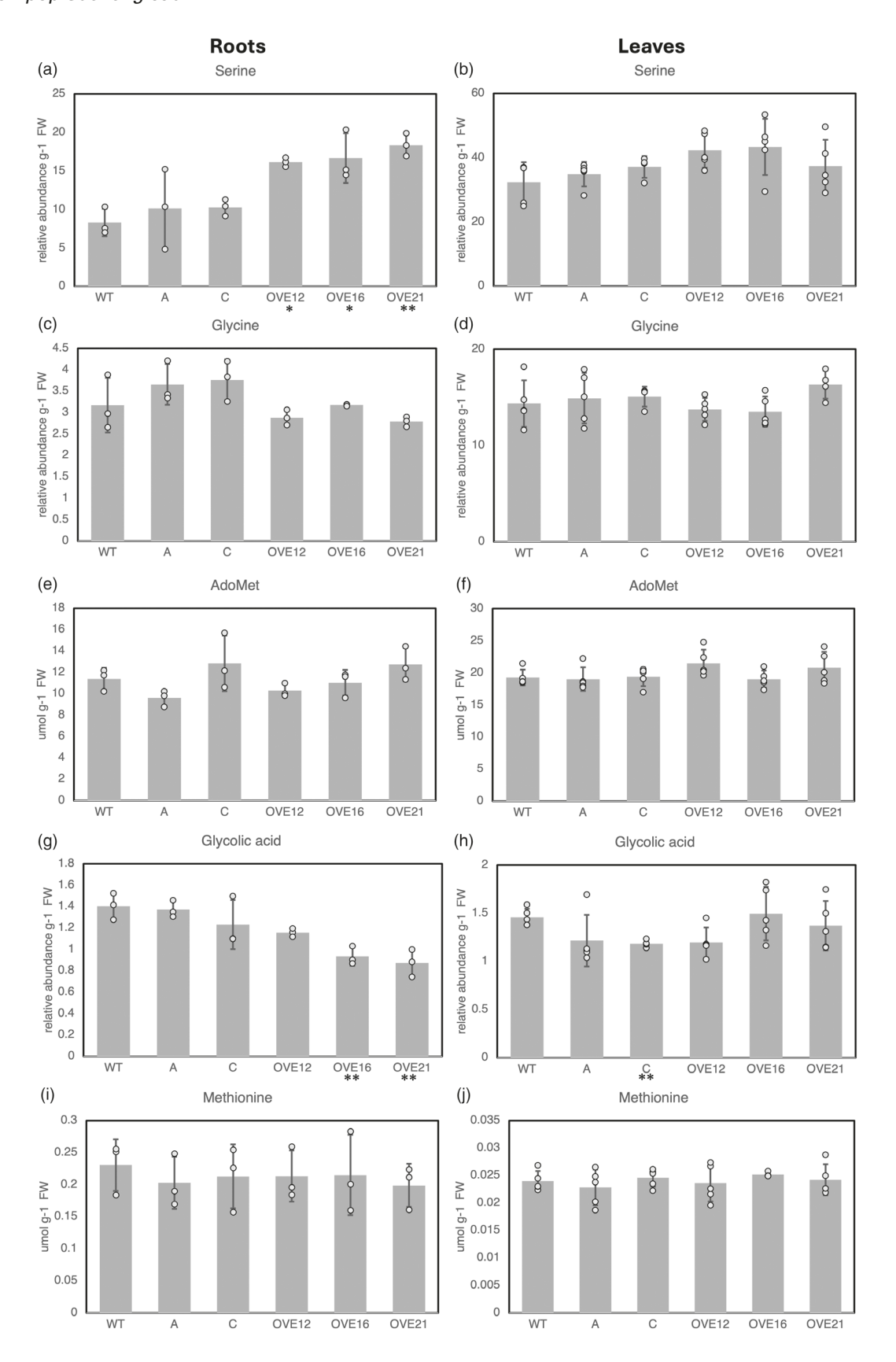
This study provides data confirming that AtFTHFL catalyzes the ATP-dependent conversion of formate to 10-formyl-H-4PteGlun, along with the kinetic parameters of the recombinant enzyme in vitro for H₄PteGlu_{1&5}, ATP, and formate. Our results show similar trends among the three substrates when H₄PteGlu₅ is used to replace H₄PteGlu₁ as a substrate: a roughly 10-fold smaller K_m values and turnover numbers (k_{cat}) . The finding of the enhanced AtFTHFL affinity toward polyglutamylated H₄PteGlu_n is in accordance with the findings in previous studies of the native FTHFL enzymes purified from rabbit liver (Strong et al., 1987) and pea cotyledons (Kirk et al., 1994). Such enhanced affinity for polyglutamylated vs. monoglutamylated folate substrates has also been found in other folate-dependent plant enzymes including 5-formyltetrahydrofolate ligase (Roje et al., 2002), the plastidial serine hydroxymethyltransferase AtSHMT3 (Zhang et al., 2010), and the cytosolic serine hydroxymethyltransferase AtSHMT4 (Wei et al., 2013). The enhanced affinity of the folate-dependent enzymes for the polyglutamylated folate species as compared to the monoglutamylated ones is caused by the binding of the glutamate tail to the enzyme (Strong et al., 1987). Unlike these other enzymes, however, which are catalytically more efficient with the pentaglutamylated substrates, catalytic efficiencies of the AtFTHFL enzyme with H₄PteGlu₁ and H₄PteGlu₅ are similar.

The GUS fusion promoter analysis shows that *AtFTHFL* is strongly expressed at the columella and lateral root cap of primary and secondary roots. Consistent with this expression pattern, *AtFTHFL* knockdown mutants have shorter roots as compared to the wild type plants (Figure 5).

With respect to the short root phenotype of the T-DNA knockdown mutants, one possibility that explains this phenotype in the AtFTHFL knockdown mutants is that formate is an important source of C1 units to non-photosynthetic tissues, and that rapidly growing root tips may require FTHFL to supply the C1 units for rapid cell growth. This provision of C1 units would not be limiting to growth, since the overexpressors did not have an increase in growth. Another possibility we cannot completely exclude is that this growth impairment in the knockdown mutants is due to formate accumulation at the root tips, consistent with a previously published study showing that formate accumulation reduced the primary root growth when the wild type seedlings were grown on MS medium with exogenously added formate (Li et al., 2002). Our measurement on the whole roots of the T-DNA knockdown mutants does show the formate contents trending upwards in the mutants as compared to the wild type plants, although the statistical analysis shows that the significance of the measurement is above our a priori alpha of 0.05. We cannot exclude the possibility that this is because our measurements were done with the whole roots instead of root tips as collecting enough root tip tissue for the formate analysis was technically challenging.

A further possibility for our observed phenotype is due to auxin signaling, which has been linked to disruptions in folate metabolism. A deletion in a gene encoding a dihydroneopterin aldolase that functions in folate biosynthesis in Arabidopsis has shown developmental defects in primary roots resulting in a reduced length as well as significant reductions in H₄PteGlu_n, dihydrofolate, and 5methyl-H₄PteGlu_n (Li et al., 2023). Further evaluation showed that folates could promote rootward auxin transport and may affect particular auxin/indole-3-acitic acid proteins and auxin response factors (Li et al., 2023). Similarly, folic acid (which can be reduced to H₄PteGlu_n via dihydrofolate) supplementation has been shown to inhibit primary root elongation and induce lateral root formation by promoting cell division while preventing cell elongation through auxin redistribution within the roots (Ayala-Rodriguez et al., 2017). While the link between AtFTHFL and the auxin pathway is beyond the scope of this study, it is a possibility and an area for future study.

Links between root development and folate metabolism have been observed in other folate pathway mutants. Folylpolyglutamate synthetases (FPGSs) catalyze the addition of glutamate residues to folate molecules. In *Arabidopsis*, impairment of the plastidial FPGS1 gene resulted in a short primary root phenotype (Reyes-Hernandez



Glycine, serine, and glycolic acid were measured using GS-MS and are presented on a relative abundance bases to a ribitol internal standard on a fresh weight basis (RA g⁻¹ FW). Methionine and AdoMet were measured using HPLC and presented on an absolute molar basis (µmol g⁻¹ FW). The data are an average of three to five experiments; error bars depict standard deviation. Asterisk indicates significant difference compared to the wild type (*P < 0.05; **P < 0.01).

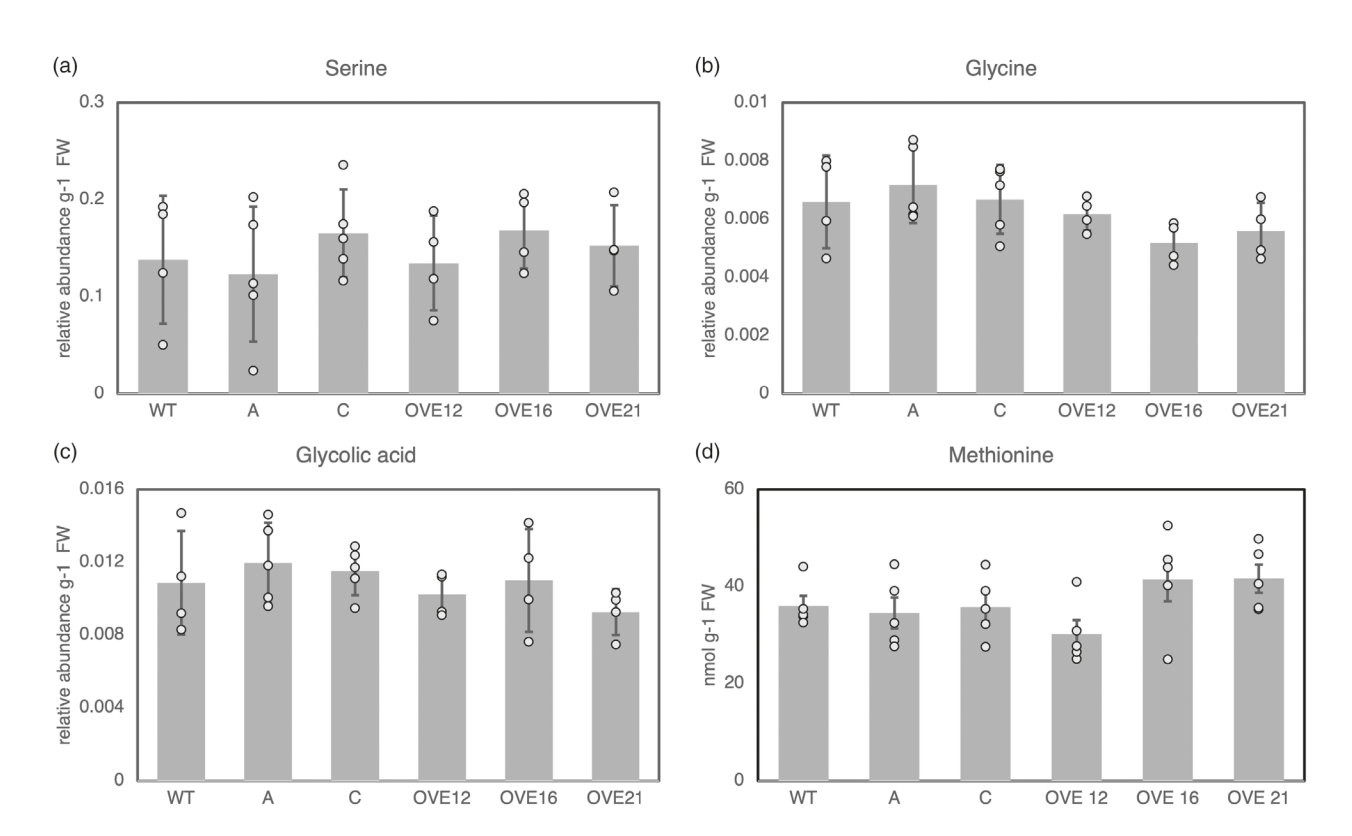


Figure 11. Serine (a), glycine (b), glycolic acid (c), and methionine (d) in leaves of plants grown under elevated CO2 (2000 PPM) of the two T-DNA insertion lines (A and C), the three overexpressor lines (OVF12, OVF16 and OVF21), and the wild type (WT) plants Glycine, serine, and glycolic acid were measured using GC-MS and are presented on a relative abundance basis to a ribitol internal standard on fresh weight basis (RA g⁻¹ FW). Methionine was measured using HPLC and presented on an absolute molar basis (nmol g⁻¹ FW). The data are an average of three to five experiments; error bars depict standard error. Asterisk indicates significant difference compared to the wild type (*P < 0.05; **P < 0.01).

et al., 2014; Srivastava et al., 2011) as well as altered ratios of various folate species. Srivastava et al. (2011) observed significant increases in monoglutamylated 5-methyl-H₄₋ PteGlu_n, 5,10-methenyl-H₄PteGlu_n + 10-formyl-H₄PteGlu_n, and total folates in their impaired mutant compared to wild type and a decrease in polyglutamylated 5,10-methenyl-H₄-PteGlu_n + 10-formyl-H₄PteGlu_n and increase in 5-formyl-H₄-PteGlu_n in their mutant compared to wild type. We cannot speak to any differences in mono-versus polyglutamylated folate species ratios, but did observe a significant increase in 5,10-methenyl-H₄PteGlu_n + 10-formyl-H₄PteGlu_n in one of our impaired FTHFL lines (line A) and a non-significant upward trend in the other impaired line (line C). On the other hand, Reyes-Hernandez et al. (2014) observed increases in both THF and 5-formyl-H₄PteGlu_n and decreases in 5-methyl-H₄PteGlu_n in the impaired FPGS1 mutants compared to wild type, with similar patterns being

observed in both monoglutamylated and polyglutamylated folates. We did not observe a significant change in either H₄PteGlu_n or 5-methyl-H₄PteGlu_n in either impaired FTHFL line compared to wild type (and did not measure 5-formyl-H₄PteGlu_n). Conversely, overexpression of a foxtail millet FPGS gene possessing a tetrahydrofolypolyglutamate synthetase domain in Arabidopsis increased H₄PteGlu_n, 5methyl-H₄PteGlu_n, 5-formyl-H₄PteGlu_n, 5,10-methyene-H-4PteGlun, and dihydrofolate and increased root length due to the promotion of cell division in the root apical meristem (Zhang et al., 2023). We saw neither a broad increase in folates, nor increased root growth in any of our mutant lines.

It is also worth noting that in several of the aforementioned studies exogenous application of 5-formyl-H-4PteGlun can reverse the short root phenotypes seen in plants with impaired folate pathways (Li et al., 2023;

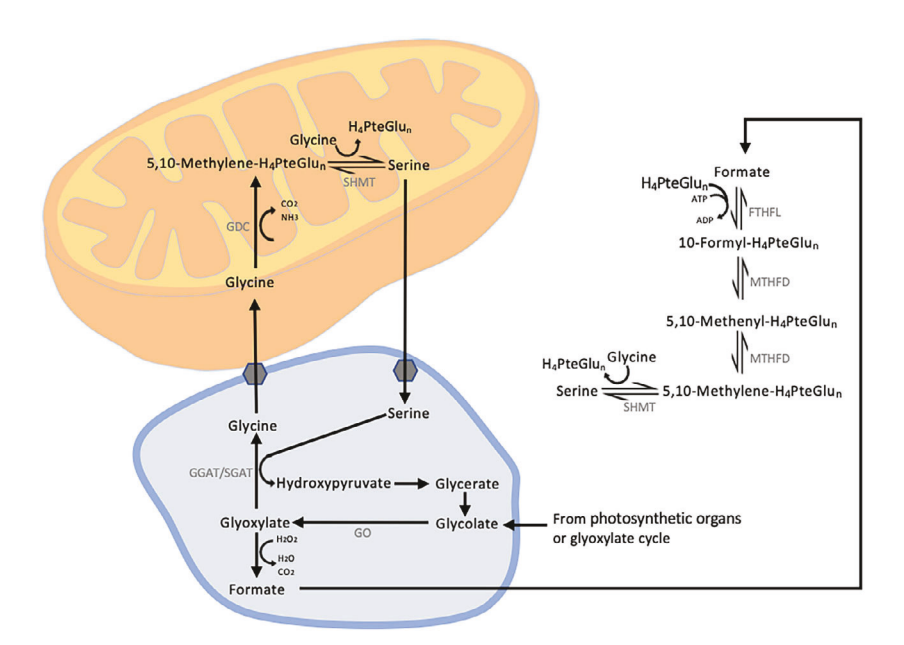


Figure 12. Hypothesized subcellular compartmentation of the C_1 metabolic network and associated reactions in plant roots. ADP, adenosine diphosphate; ATP, adenosine triphosphate; FTHFL, formyltetrahydrofolate ligase; GDC, glycine decarboxylase complexes; GGAT, glutamate: glyoxylate aminotransferase; GO, glycolate oxidase; H_4 PteGlu_n, tetrahydrofolate; MTHFD, bifunctional methylenetetrahydrofolate dehydrogenase/methenyltetrahydrofolate cyclohydrolase; SGAT, serine:glyoxylate aminotranserase; SHMT, serine hydroxymethyltransferase.

Srivastava et al., 2011) and can promote root growth alone (Lasok et al., 2023), suggesting it may act as a positive regulator of root development.

Regardless of which of the proposed mechanisms above is correct (and they do not mutually exclude each other), the observed root phenotype is consistent with the hypothesis that AtFTHFL operates in the direction of 10-formyl- H_4 PteGlu_n biosynthesis *in planta*, as previously proposed (Iwai et al., 1967a; Kirk et al., 1994). This is in contrast with the direction in which FTHFL operates in purinolytic organisms, in which it converts 10-formyl- H_4 PteGlu_n and formate (MacKenzie et al., 1984).

To find other lines of evidence supporting the hypothesis that AtFTHFL operates in the direction of 10-formyl-H-4PteGlun in planta, we investigated the relevant metabolite pool sizes in both roots and rosettes of the transgenic plants compared to the wild type controls. The overexpression of AtFTHFL resulted in the substantial reduction in formate pool size in the roots of AtFTHFL overexpression lines. In addition, H₄PteGlu_n + 5,10-methylene-H₄PteGlu_n accumulated in the roots of these lines. Although we cannot distinguish between THF and 5,10-methylene-H-4PteGlun in our analysis because 5,10-methylene-H₄PteGlun is degraded to H₄PteGlu_n during the extraction (Konings, 1999), we hypothesize that 5,10-methylene-H₄PteGlu_n rather than H₄PteGlu_n, accumulates in the roots of the AtFTHFL overexpression lines because 5,10-methylene-H-4PteGlun is downstream of 10-formyl-H4PteGlun on the onecarbon metabolic pathway (Figure 1). This result suggests that the newly formed 10-formyl-H₄PteGlu_n is rapidly processed further to 5,10-methenyl-H₄PteGlu_n and to 5,10-methylene-H₄PteGlu_n by means of the cytosolic bifunctional methylenetetrahydrofolate dehydrogenase/methenyltetrahydrofolate cyclohydrolase (MTHFD).

Production of 5,10-methylene-H₄PteGlu_n is thought to be catalyzed mainly by serine hydroxymethyltransferase, which converts serine + H₄PteGlu_n to glycine + 5,10methylene-H₄PteGlu_n, in the cytosol of plant leaves, where a large amount of serine is produced during photorespiration (Hanson & Roje, 2001). Glycolate has been proposed as a source of C₁ units for serine biosynthesis in heterotrophic plant tissues, which do not photorespire (Schmitz et al., 2020). According to this hypothesis, glycolate would either be transported to heterotrophic tissues from photosynthetic source organs or would alternatively be produced from glyoxylate formed in the glyoxylate cycle in situ. It is likely that the in situ production of glycolate predominates since glycolate is undetectable in vascular exudates of Arabidopsis or tobacco (Ma et al., 2014; Xu et al., 2021). Glycolate would then be converted in peroxisomes back to glyoxylate via glycolate oxidase, and then further to glycine via glutamate:glyoxylate aminotransferase/serine:glyoxylate aminotransferase. This glycine would then enter mitochondria and would be used there for the biosynthesis of serine and 5,10-methylene-H₄PteGlu_n via the reactions catalyzed by serine hydroxymethyltransferase and glycine decarboxylase (Figure 12).

Our results showing elevated serine and reduced glycolate pool sizes in the roots of the AtFTHFL overexpressors as compared to the wild type plants (Figure 10) strongly support the hypothesis that glycolate is used for serine biosynthesis in heterotrophic tissues. Since our overexpressors have elevated cytosolic FTHFL activity, we propose that at least some of the root glyoxylate pool is non-enzymatically decarboxylated to formate, which is then funneled into the C₁ metabolic network via the cytosolic FTHFL. The formed 10-formyl-H₄PteGlu_n would then be sequentially reduced to 5,10-methenyl-H₄PteGlu_n and 5,10-methylene-H₄PteGlu_n. Finally, the cytosolic serine hydroxymethyltransferase, operating in the opposite direction from that in which it operates in the leaves, would convert 5,10-methylene-H₄PteGlu_n and glycine to serine. The lack of change in the pool sizes of 5-methyl-H₄PteGlu_n, methionine, and S-adenosylmethionine (AdoMet) is consistent with the extra 10-formyl-H₄PteGlu_n produced in the AtFTHFL overexpressors providing its C₁ unit mainly for serine biosynthesis, and not for the biosynthesis of 5methyl-H₄PteGlu_n, methionine, and AdoMet. Leaves of the overexpression lines lacked the metabolite changes observed in the roots under ambient conditions, suggesting that FTHFL is not a major player in terms of regulating the flux of C_1 units through the core C_1 metabolism in green tissues. Low flux of C₁ units in leaf tissue through non-enzymatic decarboxylation of glyoxylate is supported in mutants lacking catalase, but more formal flux work involving labeled intermediates is needed to confirm this (Bao et al., 2021).

In summary, our results support the hypothesis that the physiological role of AtFTHFL is to feed cellular formate primarily in roots, some of which is most likely originating from glycolate through glyoxylate and then nonenzymatic decarboxylation to formate, into the C₁ metabolism, and that the increased flux of C₁ units through this enzyme is mainly used by the cytosolic serine hydroxymethyltransferase for serine production, but not so much by the methylenetetrahydrofolate reductase for the production of 5-methyl-H₄PteGlu_n. This finding has an important implication for any attempts to increase the flux of C₁ units into methylated metabolites in heterotrophic organs such as roots and tubers by engineering the cytosolic C₁ metabolism as it suggests that increasing activity of any cytosolic C₁ enzyme downstream of the methylenetetrahydrofolate reductase (Figure 1) is likely to lead to a perturbation in serine to glycine conversion in the cytosol rather than to an increase in the flux through methylenetetrahydrofolate reductase and then onwards to S-adenosylmethionine and the methylated products.

METHODS

Identification of the candidate gene for AtFTHFL and recombinant expression of the encoded protein

The candidate gene for AtFTHFL had been previously identified based on sequence homology to its bacterial, yeast, and

mammalian counterparts (Iwai et al., 1967b; Mejillano et al., 1989; Walkup & Appling, 2005) but the encoded enzyme remained biochemically uncharacterized until this study. To investigate function of the putative AtFTHFL, the full-length cDNA clone for AtFTHFL (stock#U15996) was ordered from Arabidopsis Biological Resource Center (ABRC). The primers FTFHL_F and FTHFL_R (Table S1) were employed to amplify the cDNA and subclone it into pET-30 EK/LIC following the manufacturer's protocols. The pET30-AtFTHFL vector was sent to Eurofins Genomics for sequencing to confirm that the cDNA was in frame and error free. The pET30-AtFTHFL vector was then transformed into the *E. coli* expression strain BL21 (DE3), and the bacteria were grown in the Luria-Bertani medium containing 100 mg mL⁻¹ kanamycin at 37°C until the OD₆₀₀ reached 0.6. The recombinant protein expression was then induced by adding isopropyl β-thio-glactopyranoside to obtain the final concentration of 1 mM. The induced culture was grown at 15°C for 16 h. Bacterial cells were then harvested by centrifugation at 5500 rpm for 15 min at 4°C, and the cell pellet was resuspended in the extraction buffer (25 mM Tris-HCl pH 7.5, 10 mM Imidazole, 1 mM MgCl₂, 400 mM KCl, 10% glycerol, 10 mM β-mercaptoethanol, and 1 mM PMSF). The bead beating technique was employed to break the cells by using Mini Beadbeater-8 (Biospec, OK). Supernatant containing the soluble recombinant protein was collected after centrifuging the crude extract at 14 000 rpm for 20 min at 4°C.

The recombinant AtFTHFL protein containing an N-terminal hexahistidine tag was purified on a nickel-charged HiTrap IMAC column using an AKTA FPLC system (GE Healthcare, NJ). The IMAC column was equilibrated with binding buffer (25 mM Tris-HCl pH 7.5, 10 mM lmidazole, 1 mM MgCl₂, 400 mM KCl, 10% glycerol and 10 mM β-mercaptoethanol). The recombinant AtFTHFL was eluted using elution buffer (25 mM Tris-HCl pH 7.5, 500 mM Imidazole pH 7.5, 1 mM MgCl₂, 400 mM KCl, 10% glycerol, and 10 mM β-mercaptoethanol) over a gradient from 10 to 500 mM imidazole. The recombinant protein eluted at around 150 mM imidazole. The fractions containing the recombinant AtFTHFL protein were pooled and desalted using a disposable PD 10 desalting column (GE Healthcare, NJ), which had been equilibrated with desalting buffer (25 mM Tris-HCl pH 7.5, 2.5 mM MgCl2, 200 mM KCI, 10% glycerol, and 10 mM β-mercaptoethanol). SDS-PAGE analysis of the purified protein showed a single band at approximately 70 kDa, as expected (Figure S1).

The N-terminal hexahistidine tag was then removed by incubating with 0.1 U mL⁻¹ of Recombinant Enterokinase (Novagen) at 30°C for 4 h. The untagged recombinant AtFTHFL was repurified on a nickel-charged HiTrap IMAC column following the earlier procedure and eluted in the flow-through. Fractions containing the untagged recombinant AtFTHFL were desalted using a disposable PD 10 desalting column, which had been equilibrated with desalting buffer (100 mM Triethanolamine HCl buffer pH 7.5, 2.5 mM MgCl₂, 200 mM KCl, 10% glycerol, and 10 mM βmercaptoethanol). Protein concentrations were quantified using the Quick Start™ Bradford Protein Assay (Bio-Rad, CA) and bovine serum albumin as the standard. The untagged enzyme displayed a band at approximately 67-kDa on an SDS-PAGE gel, as expected (Figure S1).

Synthesis of pentaglutamylated H₄PteGlu_n

Pteroylpenta-gamma-L-glutamic acid was chemically reduced by potassium borohydride (KBH₄) to produce H₄PteGlu₅ using a published procedure (Scrimgeour & Vitols, 1966). The H₄PteGlu₅ was purified on a Mono Q 5/50 GL column. Bound folates were eluted using a linear gradient of 0.13-2 M Sodium acetate, pH 6.9

containing 0.2 M β-mercaptoethanol. The eluate fractions were collected over 20 column volumes following Besson et al. (1993). The H₄PteGlu₅ was further purified with solid phase extraction on a Chromabound C₁₈ Hydra column (Macherey-Nagel, Duren, Germany). After the H₄PteGlu₅ was loaded onto the column, the column was washed with methanol and water respectively. The H₄PteGlu₅ was eluted with 10 mM Tris(3-hydroxypropyl) phosphine and all the fractions were combined and stored at -80°C until use.

FTHFL enzyme assay

The enzyme activity of AtFTHFL was investigated using a previously published procedure (Kirk et al., 1994) with some modifications. The enzyme assay was performed by incubating 12.5 µL of untagged recombinant AtFTHFL with 37.5 µL of buffer A (100 mM Triethanolamine HCl buffer pH 7.5, 2.5 mM MgCl₂, 200 mM KCl, 10% glycerol, 10 mM β-mercaptoethanol, 100 mM ammonium formate, 1 mM H₄PteGlu_n, and 2 mM ATP) at 30°C for 10 min. The enzymatic reaction was terminated by adding 100 µL of 0.37 M HCI, which acidified the reaction and converted the 10-formyl-H-4PteGlun product of the reaction to 5,10-methenyl-THF. The HPLC with fluorescence detection was then used for improved sensitivity instead of spectrophotometry to measure the produced 5,10methenyl-H₄PteGlu_n. 5,10-methenyl-H₄PteGlu_n was separated isocratically on an Xterra C18 Column (4.6 \times 100 mm, 5 $\mu m)$ and was monitored with 360 nm excitation and 460 nm emission wavelengths. The mobile phase contained 27 mM phosphoric acid and the flow rate was 0.8 mL min⁻¹. Authentic 5,10-methenyl-H-4PteGlun was purchased from Schircks Laboratories (Jona, Switzerland) and it was used as standard for quantification.

Determination of subcellular localization

A coding sequence of AtFTHFL was PCR-amplified from the cDNA clone (stock#U15996) using specific primers (attB-FTHFL F and attB-FTHFL_R, Table S1) with Phusion High-Fidelity DNA polymerase (New England Biolabs, MA). The resulting PCR product was cloned into the Gateway pDOR221 entry vector, using BP Clonase[™] II enzyme mix (Invitrogen, CA). The AtFTHFL was subsequently moved into the destination vectors pK7FWG2 (C-terminal EGFP tag) and pK7WGF2 (N-terminal EGFP tag) using the LR Clonase™ II enzyme mix (Invitrogen, CA). Each construct was transformed into the Agrobacterium tumefaciens strain GV3101 using electroporation, and then into Arabidopsis using the floral dip method (Clough & Bent, 1998). The transformants were selected on MS media supplemented with 50 µg mL⁻¹ of kanamycin. Leaves of the stable transformants expressing the AtFTHFL-EGFP and AtFTHFL-EGFP were mounted in water and imaged using a Leica SP8 confocal laser scanning microscope with 488 nm excitation and 495-530 nm emission.

Generation of stable transgenics containing the GUSpromoter fusion

To create the pFTHFL::GUS constructs, two primers with attB sequences for Gateway cloning (FTHFL-GUS_F and FTHFL-GUS_R; Table S1) were used to amplify the 1535-bp region upstream of AtFTHFL cDNA with Phusion High-Fidelity DNA polymerase (New England Biolabs, MA). The resulting PCR product was subcloned into the pDOR207 entry vector using BP ClonaseTM II enzyme mix (Invitrogen, CA) and subsequently transferred into the binary pKGWFS7 vector containing the glucuronidase (GUS) reporter gene using the LR ClonaseTM II enzyme mix (Invitrogen, CA). All clones were verified to be error-free and in frame by sequencing as before. The vector was then transformed into the Agrobacterium strain GV3101 using electroporation. The floral dip method was employed to introduce the pFTHFL::GUS construct into Arabidopsis as previously described. The transgenic seeds were screened on MS medium containing 40 μg mL⁻¹ of kanamycin. Three independent T3 generation homozygous lines were employed for examining spatiotemporal activity of AtFTHFL promoter.

Histochemical GUS staining

GUS histochemical staining of the transgenic Arabidopsis plants containing the AtFDH::GUS fusion construct was conducted following the previously described procedure (Jefferson, 1987). The GUS staining buffer consisted of 50 mM phosphate buffer, 2 mM potassium ferrocyanide, 2 mM potassium ferricyanide, and 2 mM X-Gluc (5-Bromo4-Chloro-3-Indolyl-Beta-D-Glucuronide) (Gold Biotechnology, USA). The plant tissues were incubated in the GUS staining solution at 37°C for 16 h.

Generation and screening of the transgenic knockdown and overexpressor plants

Arabidopsis ecotype Columbia (Col-0) was used throughout this study as a control. Two T-DNA insertion lines, Salk_054151(A) and Salk _067510 (C), were obtained from the Arabidopsis Biological Resource Center (ABRC). To screen for the T-DNA insertions, genespecific primers (SS004_R for line A and SS003_R for line C, Table S1) in combination with the T-DNA left border primer (LBb1.3) were used. The homozygous AtFTHFL T-DNA insertion lines were confirmed by a pair of gene-specific primers (SS004_F and SS004_R for line A; SS003_F and SS003_R for line C, Table S1).

To generate overexpression transgenic Arabidopsis lines, a coding sequence of AtFTHFL was PCR-amplified from the cDNA (stock#U15996) using gene specific primers (attB-FTHFL_F and attB-FTHFL_R, Table S1) with Phusion High-Fidelity DNA polymerase (New England Biolabs, MA). The resulting PCR product was cloned into the Gateway pDOR221 entry vector, using BP Clonase $^{\text{\tiny TM}}$ II enzyme mix (Invitrogen, CA). Using the LR Clonase™ II enzyme mix (Invitrogen, CA), the AtFTHFL was subsequently cloned into the destination vector pB2GW7, for expression under control of the Cauliflower mosaic virus (CaMV) 35S promoter. All the constructs were sent to Eurofins Genomics for DNA sequencing to confirm that the sequences were error free. AtFTHFL-pD2GW7 plasmid was then transformed into the A. tumefaciens strain GV3101 using electroporation. The floral dip method was employed to transform Agrobacterium carrying the AtFTHFL-pD2GW7 plasmid into the Arabidopsis wild type plants (McCormac et al., 1998). The seeds collected from the transformed plants were germinated in soil and sprayed with BASTA (glufosinate ammonium) (120 mg L⁻¹) to select for the T_1 transgenic plants. The T_2 and T_3 progeny were sequentially re-screened with BASTA, and seeds collected from the survivors. The seeds collected from the T3 generation transgenics were planted on MS medium with 15 mg L⁻¹ of BASTA to test for homozygosity. Plants that produced the seed showing 100% survival on MS medium with 15 mg L^{-1} of BASTA were considered homozygous and used in the downstream experiments.

The most severe knockdown (Line C) was complemented by crossing it with the overexpressor with the highest expression level (OVE21). This double mutant was allowed to self-cross, and its progeny were screening using the methods listed above.

Gene expression analysis

Seedlings of all transgenic lines and the wild type were grown on vertical plates containing a half-strength Murashige and Skoog (MS) medium. The shoots and roots of seedlings were separately collected and pulverized in liquid nitrogen. RNA isolation was performed using the RNeasy Plant Mini Kit (Qiagen) with DNase I digestion to remove any contaminating DNA. The total RNA concentration was determined using a NanoDrop spectrophotometer. An equal amount of RNA in each sample was reverse-transcribed to cDNA using the ProScript® II First Strand cDNA Synthesis Kit (NEB, MA). Three technical replicates were run, and cycle threshold values were measured with the Applied Biosystems 7500 Fast Thermal Cycler. Real-time PCR was performed using Platinum Taq DNA polymerase (Invitrogen, CA). SYBR Green was used to monitor dsDNA synthesis in an optical 96-well plate. Gene specific primers (qFTHFL_F and qFTHFL_R, Table S1) were used to amplify the AtFTHFL cDNA, and actin 2 primers (qACTIN2_F and qAC-TIN2_R, Table S1) were employed for data normalization (Czechowski et al., 2005).

Determination of FTHFL enzyme activity in plant extracts

Seedlings of all transgenic lines and the wild type were grown on vertical plates containing half-strength Murashige and Skoog (MS) medium. The shoots and roots of seedlings were separately collected and pulverized in liquid nitrogen. An extraction buffer (100 mM Triethanolamine HCl buffer pH 7.5, 2.5 mM MgCl₂, 200 mM KCl, 10% glycerol, 1 mM PMSF, and 10 mM β mercaptoethanol) was added to the ground leaves in a 1.5 mL tube and the tube was centrifuged at 13 500 rpm for 5 min at 4°C. Only the clear supernatant was loaded into the 0.5 mL ZebaTM Spin Desalting Columns (Thermo Scientific, IL), which had been equilibrated with the extraction buffer. The desalted extracts were assayed for FTHFL activity as described above. Protein concentrations of plant extracts were quantified using the Quick Start™ Bradford Protein Assay (Bio-Rad, CA) and bovine serum albumin as the standard.

Growth conditions for the metabolite analyses

To obtain uniform germination, all Arabidopsis seeds were imbibed at 4°C with distilled water for 2 days before planting. Growth conditions were as follows unless otherwise specified: 20°C during the day and 18°C during the night, 70%-80% humidity, and a 12-h-light/12-h-dark cycle with the light intensity of 120 mmol photon m⁻² sec⁻¹. For the metabolite analyses, we used plate-grown seedlings for collecting root tissues and soilgrown plants for shoot tissues. The soil-grown plants were grown both under ambient air and elevated CO₂ (2000 ppm) conditions. Roots were collected from seedlings grown on vertical halfstrength Murashige and Skoog (MS) medium plates, which were placed randomly in a growth chamber. To account for any effects of root tissue exposed to light while growing on plates, a second set were grown with the root portions shielded from light. All tissues were pulverized in liquid nitrogen after the harvest and stored at -80°C until analysis.

Phenotype analyses

For root phenotype analyses, Arabidopsis seeds were surfacesterilized with 30% (v/v) commercial bleach containing 0.02% triton X-100. The sterilized seeds were placed on the half MS medium and kept in a dark room at 4°C for 2 days. After stratification, the seeds were plated on the MS plates and were grown vertically at 100-150 mmol photon m⁻² sec⁻¹, 22°C, with 9 h light and 15 h dark cycle. Once germinated, the seedlings were transferred to 120 imes 120 mm plates with half MS media. The seedlings were placed back into the growth chamber and grown on vertically placed plates for 2 days, at which point the position of each

root tip was marked. The seedlings were then grown for another 7 days. Following this growth period, the plates were imaged using a digital scanner. Root length and lateral root density (as defined as the number of lateral roots divided by the length of the root branching zone) on the plate scans were measured using the ImageJ software (National Institutes of Health).

Additionally, we also examined the length of the tap root meristems of the knockdown and wild type lines. Plants for this analysis were germinated for 5 days on half MS media plates. The plants were then transferred to glass slides and imaged using a Leica DMI300B inverted microscope. Meristem length was then measured using the ImageJ software.

For phenotypic analyses of the aerial parts, Arabidopsis plants were grown under long days (16 h-light cycle) with 120 mmol photon m⁻² sec⁻¹, at the temperature of 22°C during the day and 20°C during the night. The flowering time was monitored by counting the number of days from sowing the seeds until the first flower buds are visible (Stage 5.1) (Boyes, 2001). The height of plants was measured at stage 6.5 (Boyes et al., 2001). Each plant rosette at stage 6.5 was weighed individually for the fresh weight. Next, the plant rosettes were frozen and lyophilized before weighing again to obtain the dry weight.

Folate analysis

Folate analysis was conducted essentially as before (Hung et al., 2013). One milliliter of folate extraction buffer (50 mM CHES-50 mM HEPES buffer, pH 7.9 containing 1 mM CaCl₂, 2% (w/v) Na-ascorbate, and 10 mM β-mercaptoethanol) was added to approximately 100 mg of pulverized tissue. Subsequently, the sample was boiled for 10 min and only the supernatant was collected after centrifuging the sample at 14 000 rpm, 4°C. The pellet was re-extracted with 1 mL of the folate extraction buffer and the supernatants were combined. The extract was deglutamylated by adding 100 µL of dialyzed rat plasma (Konings, 1999) and incubating at 37°C for 4 h. The extract was subsequently boiled for 15 min to deactivate the enzymes in rat plasma and the denatured proteins were precipitated by centrifuging for 20 min at 14 000 rpm, 4°C.

The clear supernatant was obtained by filtering the extract through a 0.45 mm PVDF filter (National Scientific, TN). The clear supernatant was applied to the folate-binding column, which was prepared following a published procedure (Konings, 1999). Folates were eluted from the column by applying 0.5 mL of HPLC mobile phase (Eluent B, 28 mM K₂HPO₄ and 60 mM H₃PO₄ [pH 2.5]) containing 1% ascorbic acid. Elution was carried out following a gradient procedure (Table S2). The Alliance® HPLC System (2695 Separations Module, Waters, MA) with fluorescence detection (2475 Multi-Wavelength Fluorescence Detector, Waters) and the Cadenza CD-C18 column (3 mm, 4.6 \times 250 mm, Imtakt Co., Japan) was employed to analyze the folates. Folates were quantified using standards of authentic H₄PteGlu₁, 5,10-methenyl-H₄PteGlu₁, and 5-methyl-H₄PteGlu₁ (Schicks Laboratories, Jona, Switzerland).

Amino acid, AdoMet and formate analyses

The samples designated for amino acid, AdoMet, and formate analyses were treated as follows. To prepare samples for HPLC measurements, approximately ~80 mg of frozen leaf samples were ground under cryogenic conditions using a mortar and pestle with liquid N₂. For each sample, 10 μL of 10 mM amino butyric acid (ABA) was added as an internal control into 0.25 mL of 0.1 M HCI. This mixture was subsequently added to approximately 100 mg of pulverized shoot tissue. The samples were then centrifuged for 20 min at 14 000 rpm at 4°C. The supernatant was

collected, and the pellet was re-extracted with 0.25 mL of 0.1 M HCI. The supernatants were combined before further analysis.

For amino acid analysis, the samples were derivatized using the AccQTag reagent (AccQ-Fluor Reagent kit, Water, MA) as described by the manufacturer. The derivatized samples were separated on a AccQTag column (3.9 \times 150 mm, Waters, MA) linked to the Alliance[®] HPLC System (2695 Separations Module, Waters, MA) with fluorescence detection (2475 Multi-Wavelength Fluorescence Detector, Waters). The Eluent A (ultrapure water) and Eluent B (acetonitrile), and Eluent D (200 mL AccQTag Ultra Eluent A Concentrate mixed with 2 L ultrapure water) from Waters were used for the separation using a gradient procedure (Table S3) with the fluorescence detection at 395 nm for absorption and 254 nm for excitation. Amino acids were quantified using commercial amino acid mixtures (A2161 and A6407, Sigma, MO) as the standards.

AdoMet analysis was conducted using a published procedure (Rzewuski et al., 2007) with the following modifications. To 15 µL of each sample was added 49 µL of 0.48 M citrate/0.59 M phosphate buffer pH 4.0, and 36 µL of chloroacetaldehyde (Sigma, MO). The resulting samples were incubated at 80°C for 10 min. The derivatized samples were immediately transferred to ice and subsequently centrifuged at 14 000 rpm for 1 h, 4°C. The Xterra MS C₁₈ column (5 mm, 4.6×100 mm, Waters, MA) with mobile phase Eluent A (TBAS buffer; 5.7 mM tetrabutylammonium hydrogen sulphate, 30.5 mM KH₂PO₄, pH 5.8, adjusted with KOH); and Eluent B (TBAS buffer and acetonitrile in ratio of 1:2 (v/v)) were used for the separation using the gradient procedure shown in Table S4. Fluorescence detection at 410 nm, and excitation at 280 nm were applied to detect the derivatized AdoMet in the samples. Pure S-(5'-Adonosyl)-L-methionine chloride (Sigma, MO) was used as a standard to quantify the amount of AdoMet in the samples.

Formate contents were quantified following a published procedure (Xie et al., 2012) with some modifications. 50 µL of plant extract in 0.1 M HCl was combined with 50 µL of 20 mM tetrabutylammonium bromide in acetonitrile, 50 µL of 5% triethanolamine in acetone, and 1 µL of 10 mM 9-chloromethyl anthracene as a fluorescence-labeling reagent. The reaction volume was adjusted to 500 μL with acetonitrile and the reactions were incubated at 75°C for 50 min. To precipitate the debris, the samples were then centrifuged at 14 000 rpm for 10 min at 25°C. The samples were separated on the Xterra MS C_{18} column (3.5 mm, 4.6 \times 100 mm, Waters, MA) isocratically with a 1.0 mL min⁻¹ flow rate, with a mobile phase consisting of 64% acetonitrile and 36% water. Quantification was based on a comparison with the standards obtained by derivatizing pure formic acid (Sigma, MO).

To prepare samples for GC-MS measurements, approximately ~80 mg of frozen leaf samples were ground under cryogenic conditions using a FastPrep-24 instrument with CoolPrep Adapter (MP biomedicals, USA). Metabolites were extracted using a modification of the method described in Lunn et al. (2006). Briefly, samples were extracted in 500 µL pre-cooled chloroform/methanol (3:7 v/v) extraction buffer and incubated at -20°C with occasional mixing. Water soluble metabolites, including amino acids, were extracted from the chloroform phase by adding 400 μ L of UPLC-grade water and warming to 4°C with repeated shaking. Samples were then centrifuged at full speed (15 000 rpm) for 10 min at 4°C. The upper aqueous methanol-water phase was recovered for GC-MS. 200 µL of extracts were freeze dried and derivatized as described previously in Fu et al. (2022) with ribitol as the internal standard.

In preparation for GC-MS analysis, the freeze dried extract was derivatized for a 12 h at 40°C with 50 μL of 20 mg mL⁻¹ methoxyamine hydrochloride in pyridine, followed by a 60 min treatment with 50 µL N,O-Bis(trimethylsilyl) trifluoroacetamide with 1% (w/v) trimethylchlorosilane and incubated at 60°C for 60 min. Aliquots of the derivatized sample (1 μL) were injected in splitless mode with a helium carrier gas flow set at 1 mL min⁻¹, and analyzed by an Agilent 7890A GC (Agilent, USA) equipped with a 30 m VF-5 ms column and interfaced to an Agilent 5975C inert XL Mass Selective Detector (Agilent, Santa Clara, CA, USA). The GC-MS conditions were exactly as described previously in Xu et al. (2021). MSD ChemStation Data Analysis (Agilent) was used for GC-MS data acquisition, and chromatographic peaks were integrated using the MassLynx software version 4.2 (Waters). Chromatographic peaks were identified based on the retention time of authentic standard peaks and the corresponding MS spectrum.

CO₂ assimilation measurements

Gas exchange was measured on the youngest fully expanded leaves of 4- to 5-week-old plants using a LI-COR 6800 infra-red gas analyzer with the 6 cm² measuring head (LI-COR Biosciences, Lincoln Nebraska, USA). For each measurement, leaves were clamped into the gas analyzer while in the growth chamber and data were logged after standard stability definitions were satisfied, usually in 2-4 min. Since the leaves did not fully cover the chamber, the leaf area in the chamber was traced following each measurement and a picture was taken and analyzed to correct for leaf area. Leaf temperature was controlled to 20°C, irradiance of 110 μmol quanta m⁻² sec⁻¹, reference cell 400 mmol mol⁻¹, sample cell flow to 600 mmol sec⁻¹, and vapor pressure deficit to 1.5 kPa.

Statistical analysis methods

All statistical analyses were performed using RStudio statistical software (R core team) using an a priori alpha of 0.05. Assumptions of normal distribution and homogenous variance were tested using Shapiro-Wilk and Bartlett tests. Comparisons where these assumptions were met were analyzed using t-tests or an ANOVA with Tukey HSD post-hoc tests. When these assumptions were not met, these comparisons were evaluated using Wilcoxon rank sum tests or a Kruskal-Wallis with post-hoc Dunn tests.

ACKNOWLEDGEMENTS

This research was supported by the grants from NSF to S.R. (MCB-2015828) and B.W (MCB-2015843).

CONFLICT OF INTEREST STATEMENT

The authors declare no conflict of interest.

DATA AVAILABILITY STATEMENT

All data can be obtained from the manuscript and supplementary data.

SUPPORTING INFORMATION

Additional Supporting Information may be found in the online version of this article.

Figure S1. Purification of the recombinant AtFTHFL from Escherichia coli cells.

Figure S2. Dependence of the AtFTHFL activity on substrate concentration for H₄PteGlu₁, H₄PteGlu₅, ATP, and formate.

Figure S3. T-DNA insertion lines in Arabidopsis thaliana.

- **Figure S4.** The characterization of growth and development phenotype of AtFTHFL transgenic plants under standard conditions.
- Figure S5. Meristem images of wild type and knockout line C roots.
- Figure S6. Quantitative analysis of the primary root lengths of 7-day-old seedlings was conducted on the T-DNA insertion line C, the complementation cross of line C with OVE21, and the wild type plants.
- **Figure S7.** Serine and glycine in roots of plants grown in the dark of the two T-DNA insertion lines, the three overexpressor lines, and the wild type plants.
- Figure S8. CO_2 assimilation measurement of wild type and AtFTHFL transgenic plants.
- Table S1. List of primers used in this study.
- Table S2. Gradient elution system used for analysis of folates.
- Table S3. Gradient elution system used for analysis of AccQ-amino acids.
- Table S4. Gradient elution system used for analysis of AdoMet.

REFERENCES

- Atkins, C.A., Smith, P. & Storer, P.J. (1997) Reexamination of the intracellular localization of de novo purine synthesis in cowpea nodules. *Plant Physiology*, 113, 127–135.
- Ayala-Rodriguez, J., Barrera-Ortiz, S., Ruiz-Herrera, L. & Lopez-Bucio, J. (2017) Folic acid orchestrates root development linked cell elongation with auxin response and acts independently of the TARGET OF RAPA-MYCIN signaling in *Arabidopsis thaliana*. Plant Science, 264, 168–178.
- Bao, H., Morency, M., Rianti, W., Saeheng, S., Roje, S., Weber, A.P. et al. (2021) Catalase protects against nonenzymatic decarboxylations during photorespiration in *Arabidopsis thaliana*. Plant Direct, 5, e366.
- Basset, G., Quinlivan, E.P., Ziemak, M.J., de la Garza, R.D., Fischer, M., Schiffmann, S. et al. (2002) Folate synthesis in plants: the first step of the pterin branch is mediated by a unique bimodular GTP cyclohydrolase I. Proceedings of the National Academy of Sciences, 99, 12489–12494.
- Bauwe, H. & Kolukisaoglu, Ü. (2003) Genetic manipulation of glycine decarboxylation. Journal of Experimental Botany, 54, 1523–1535.
- Besson, V., Rebeille, F., Neuburger, M., Douce, R. & Cossins, E.A. (1993) Effects of tetrahydrofolate polyglutamates on the kinetic parameters of serine hydroxymethyltransferase and glycine decarboxylase from pea leaf mitochondria. *Biochemical Journal*, 292(2), 425–430.
- Boyes, D.C., Zayed, A.M., Ascenzi, R., Mccaskill, A.J., Hoffman, N.E., Davis, K.R. et al. (2001) Growth stage-based phenotypic analysis of Arabidopsis: a model for high throughput functional genomics in plants. The Plant Cell, 13, 1499–1510.
- Boyes, D.C., Zayed, A.M., Ascenzi, R., McCaskill, A.J., Hoffman, N.E., Davis, K.R. & Gorlach, J. (2001) Growth stage–based phenotypic analysis of Arabidopsis: a model for high throughput functional genomics in plants. The Plant Cell, 13(7), 1499–1510.
- Busch, F.A., Sage, R.F. & Farquhar, G.D. (2018) Plants increase CO₂ uptake by assimilating nitrogen via the photorespiratory pathway. *Nature Plants*. 4. 46–54.
- Chen, L., Chan, S.Y. & Cossins, E.A. (1997) Distribution of folate derivatives and enzymes for synthesis of 10-formyltetrahydrofolate in cytosolic and mitochondrial fractions of pea leaves. *Plant Physiology*, 115, 299–309.
- Clough, S.J. & Bent, A.F. (1998) Floral dip: a simplified method for Agrobacterium-mediated transformation of Arabidopsis thaliana. The Plant Journal, 16, 735–743.
- Cossins, E.A. (1987) Folate biochemistry and the metabolism of one-carbon units. In: Danvis, D.D. (Ed.) *The Biochemistry of plants: a comprehensive treatise*. New York: Academic Press.
- Czechowski, T., Stitt, M., Altmann, T., Udvardi, M.K. & Scheible, W.-R. (2005) Genome-wide identification and testing of superior reference genes for transcript normalization in Arabidopsis. *Plant Physiology*, 139, 5–17.
- Dirk, L.M., Williams, M.A. & Houtz, R.L. (2001) Eukaryotic peptide deformylases. Nuclear-encoded and chloroplast-targeted enzymes in Arabidopsis. *Plant Physiology*, 127, 97–107.

- Dorokhov, Y.L., Sheshukova, E.V. & Komarova, T.V. (2018) Methanol in plant life. Frontiers in Plant Science, 9, 1623.
- Douce, R., Bourguignon, J., Neuburger, M. & Rébeillé, F. (2001) The glycine decarboxylase system: a fascinating complex. *Trends in Plant Science*, 6, 167–176.
- Fu, X., Gregory, L.M., Weise, S.E. & Walker, B.J. (2022) Integrated flux and pool size analysis in plant central metabolism reveals unique roles of glycine and serine during photorespiration. *Nature Plants*, 9, 169–178.
- Gorelova, V., Bastien, O., de Clerck, O., Lespinats, S., Rébeillé, F. & van der Straeten, D. (2019) Evolution of folate biosynthesis and metabolism across algae and land plant lineages. Scientific Reports, 9, 5731.
- Groth, M., Moissiard, G., Wirtz, M., Wang, H., Garcia-Salinas, C., Ramos-Parra, P.A. et al. (2016) MTHFD1 controls DNA methylation in Arabidopsis. Nature Communications, 7, 11640.
- Hanson, A.D., Gage, D.A. & Shachar-Hill, Y. (2000) Plant one-carbon metabolism and its engineering. Trends in Plant Science, 5, 206–213.
- Hanson, A.D. & Gregory, J.F., III. (2011) Folate biosynthesis, turnover, and transport in plants. Annual Review of Plant Biology, 62, 105–125.
- Hanson, A.D. & Roje, S. (2001) One-carbon metabolism in higher plants. Annual Review of Plant Biology, 52, 119–137.
- Himes, R.H. & Rabinowitz, J.C. (1962) Formyltetrahydrofolate synthetase II. Characteristics of the enzyme and the enzymic reaction. *Journal of Biological Chemistry*, 237, 2903–2914.
- Hourton-Cabassa, C., Ambard-Bretteville, F., Moreau, F., de Virville, J.D., Rémy, R. & Des Francs-Small, C.C. (1998) Stress induction of mitochondrial formate dehydrogenase in potato leaves. *Plant Physiology*, 116, 627–635.
- Hung, C.-Y., Fan, L., Kittur, F.S., Sun, K., Qiu, J., Tang, S. et al. (2013) Alteration of the alkaloid profile in genetically modified tobacco reveals a role of methylenetetrahydrofolate reductase in nicotine N-demethylation. Plant Physiology, 161, 1049–1060.
- Iwai, K., Suzuki, N. & Mizoguchi, S. (1967a) The distribution of formyltetrahydrofolate synthetase in plants, and the purification and properties of the enzyme from pea seedlings. *Plant and Cell Physiology*, 8, 307– 325.
- Iwai, K., Suzuki, N. & Mizoguchi, S. (1967b) Purification and properties of formyltetrahydrofolate synthetase from spinach. Agricultural and Biological Chemistry, 31, 267–274.
- Jefferson, R.A. (1987) Assaying chimeric genes in plants: the GUS gene fusion system. Plant Molecular Biology Reporter, 5, 387–405.
- Kirk, C.D., Chen, L.F., Imeson, H.C. & Cossins, E.A. (1995) A 5,10-methylenetetrahydrofolate dehydrogenase—5,10-methenyltetrahydrofolate cyclohydrolase protein from *Pisum sativum. Phytochemistry*, 39, 1309–1317.
- Kirk, C.D., Imeson, H.C., Zheng, L.-L. & Cossins, E.A. (1994) The affinity of pea cotyledon 10-formyltetrahydrofolate synthetase for polyglutamate substrates. *Phytochemistry*, **35**, 291–296.
- Kisaki, T., Yoshida, N. & Imai, A. (1971) Glycine decarboxylase and serine formation in spinach leaf mitochondrial preparation with reference to photorespiration. *Plant and Cell Physiology*, 12, 275–288.
- Konings, E.J. (1999) A validated liquid chromatographic method for determining folates in vegetables, milk powder, liver, and flour. *Journal of AOAC International*, 82, 119–127.
- Kordic, S., Cummins, I. & Edwards, R. (2002) Cloning and characterization of an S-formylglutathione hydrolase from Arabidopsis thaliana. Archives of Biochemistry and Biophysics, 399, 232–238.
- Kunze, M. & Hartig, A. (2013) Permeability of the peroxisomal membrane: lessons from the glyoxylate cycle. Frontiers in Physiology, 4, 204.
- Lasok, H., Nziengui, H., Kochersperger, P. & Ditengou, F. (2023) Arabidopsis root development regulation by the endogenous folate precursor paraaminobenzoic acid, via modulation of the root cycle. *Plants*, 12, 4076.
- Li, R., Moore, M., Bonham-Smith, P.C. & King, J. (2002) Overexpression of formate dehydrogenase in *Arabidopsis thaliana* resulted in plants tolerant to high concentrations of formate. *Journal of Plant Physiology*, 159, 1069–1076.
- Li, Y., Luo, J., Chen, R., Zhou, Y., Yu, H., Chu, Z. et al. (2023) Folate shapes plant root architecture by affecting auxin distribution. *The Plant Journal*, 113, 969–985.
- Liu, J.J. & Ward, R.L. (2010) Folate and one-carbon metabolism and its impact on aberrant DNA methylation in cancer. Advances in Genetics, 71, 79–121.

- Lunn, J.E., Feil, R., Hendriks, J.H.M., Gibon, Y., Morcuende, R., Osuna, D. et al. (2006) Sugar-induced increases in trehalose 6-phosphate are correlated with redox activiation of ADPglucose pyrophosphorylase and higher rates of starch synthesis in Arabidopsis thaliana. Biochemical Journal, 397, 139–148.
- Ma, F., Jazmin, L.J., Young, J.D. & Allen, D.K. (2014) Isotopically nonstationary 13C flux analysis of changes in *Arabidopsis thaliana* leaf metabolism due to high light acclimation. *Proceedings of the National Academy of Sciences*, 111, 16967–16972.
- Mackenzie, R., Blakely, R. & Benkovic, S. (1984) Folates and pterins. Chemistry and Biochemistry of Folates, 1, 255–306.
- Mccormac, A., Elliott, M. & Chen, D. (1998) A simple method for the production of highly competent cells of Agrobacterium for transformation via electroporation. *Molecular Biotechnology*, 9, 155–159.
- Mejillano, M.R., Jahansouz, H., Matsunaga, T.O., Kenyon, G.L. & Himes, R.H. (1989) Formation and utilization of formyl phosphate by N10-formyltetrahydrofolate synthetase: evidence for formyl phosphate as an intermediate in the reaction. *Biochemistry*, 28, 5136–5145.
- Moreno, J.I., Martín, R. & Castresana, C. (2005) Arabidopsis SHMT1, a serine hydroxymethyltransferase that functions in the photorespiratory pathway influences resistance to biotic and abiotic stress. The Plant Journal, 41, 451–463.
- Mouillon, J.M., Aubert, S., Bourguignon, J., Gout, E., Douce, R. & Rebeille, F. (1999) Glycine and serine catabolism in non-photosynthetic higher plant cells: their role in C1 metabolism. *Plant Journal*, 20, 197–205.
- Neuburger, M., Rébeillé, F., Jourdain, A., Nakamura, S. & Douce, R. (1996) Mitochondria are a major site for folate and thymidylate synthesis in plants (*). Journal of Biological Chemistry, 271, 9466-9472.
- Niessen, M., Thiruveedhi, K., Rosenkranz, R., Kebeish, R., Hirsch, H.-J., Kreuzaler, F. et al. (2007) Mitochondrial glycolate oxidation contributes to photorespiration in higher plants. *Journal of Experimental Botany*, 58, 2709–2715.
- Pelloux, J., Rusterucci, C. & Mellerowicz, E.J. (2007) New insights into pectin methylesterase structure and function. *Trends in Plant Science*, 12, 267–277.
- Peterhansel, C., Horst, I., Niessen, M., Blume, C., Kebeish, R., Kürkcüoglu, S. et al. (2010) Photorespiration. The Arabidopsis book/American Society of Plant Biologists, 8, 1–24.
- Prabhu, V., Chatson, K.B., Abrams, G.D. & King, J. (1996) C-13 nuclear magnetic resonance detection of interactions of serine hydroxymethyltransferase with C1-tetrahydrofolate synthase and glycine decarboxylase complex activities in Arabidopsis. Plant Physiology, 112, 207–216.
- Rabinowitz, J.C. & Pricer, W.E. (1956) Formimino-tetrahydrofolic acid and methenyltetrahydrofolic acid as intermediates in the formation of N10formyltetrahydrofolic acid. *Journal of the American Chemical Society*, 78, 5702–5704.
- Reyes-Hernandez, B., Srivastava, A., Ugartechea-Chirino, Y., Shishkova, S., Ramos-Parra, P., Lira-Ruan, V. et al. (2014) The root indeterminacy-todeterminacy developmental switch is operated through a folate-dependent pathway in Arabidopsis thaliana. New Phytologist, 202(4), 1223–1236.
- Roje, S. (2007) Vitamin B biosynthesis in plants. *Phytochemistry*, **68**, 1904–1921.
 Roje, S., Janave, M.T., Ziemak, M.J. & Hanson, A.D. (2002) Cloning and characterization of mitochondrial 5-formyltetrahydrofolate cycloligase from higher plants. *Journal of Biological Chemistry*, **277**, 42748–42754.
- Ros, R., Muñoz-Bertomeu, J. & Krueger, S. (2014) Serine in plants: biosynthesis, metabolism, and functions. *Trends in Plant Science*, 19, 564–569.
- Rowe, P. (1984) Folates in the biosynthesis and degradation of purines. New York, Ny, USA: John Wiley.
- Rzewuski, G., Cornell, K.A., Rooney, L., Bürstenbinder, K., Wirtz, M., Hell, R. et al. (2007) OsMTN encodes a 5'-methylthioadenosine nucleosidase that is up-regulated during submergence-induced ethylene synthesis in rice (Oryza sativa L.). Journal of Experimental Botany, 58, 1505–1514.
- Schmitz, J., Hüdig, M., Meier, D., Linka, N. & Maurino, V.G. (2020) The genome of *Ricinus communis* encodes a single glycolate oxidase with

- different functions in photosynthetic and heterotrophic organs. *Planta*, **252**. 1–12.
- Scrimgeour, K. & Vitols, K.S. (1966) The reduction of folate by borohydride. Biochemistry, 5, 1438–1443.
- Serero, A., Giglione, C. & Meinnel, T. (2001) Distinctive features of the two classes of eukaryotic peptide deformylases1. *Journal of Molecular Biol*ogy, 314, 695–708.
- Smith, A.G., Croft, M.T., Moulin, M. & Webb, M.E. (2007) Plants need their vitamins too. Current Opinion in Plant Biology, 10, 266–275.
- Song, Z.B., Xiao, S.Q., You, L., Wang, S.S., Tan, H., Li, K.Z. et al. (2013) C1 metabolism and the C alvin cycle function simultaneously and independently during HCHO metabolism and detoxification in Arabidopsis thaliana treated with HCHO solutions. Plant, Cell & Environment, 36, 1490– 1506
- Srivastava, A., Ramos-Parra, P., Bedair, M., Robledo-Hernandez, A., Tang, Y., Sumner, L. et al. (2011) The folypolyglutamate synthetase plastidial isoform is required for postembryonic root development in Arabidopsis. Plant Physiology, 155, 1237–1251.
- Staben, C. & Rabinowitz, J. (1984) Formation of formylmethionyl-tRNA and initiation of protein synthesis. *Folates and Pterins*, 1, 457–495.
- Strong, W., Joshi, G., Lura, R., Muthukumaraswamy, N. & Schirch, V. (1987) 10-Formyltetrahydrofolate synthetase. Evidence for a conformational change in the enzyme upon binding of tetrahydropteroylpolyglutamates. The Journal of Biological Chemistry, 262, 12519–12525.
- Suzuki, N. & Iwai, K. (1974) The occurrence and properties of methylenete-trahydrofolate dehydrogenase in pea seedlings, and intracellular distribution of some folate-linked enzymes in the plant. *Journal of Nutritional Science and Vitaminology (Tokyo)*, 20, 89–96.
- Timm, S., Florian, A., Arrivault, S., Stitt, M., Fernie, A.R. & Bauwe, H. (2012) Glycine decarboxylase controls photosynthesis and plant growth. FEBS Letters, 586, 3692–3697.
- Walkup, A.S. & Appling, D.R. (2005) Enzymatic characterization of human mitochondrial C1-tetrahydrofolate synthase. Archives of Biochemistry and Biophysics, 442, 196–205.
- Wei, Z. & Roje, S. (2011) A high-performance liquid chromatography-based fluorometric method for assaying serine hydroxymethyltransferase toward serine formation. *Analytical Biochemistry*, **409**, 156–158.
- Wei, Z., Sun, K., Sandoval, F.J., Cross, J.M., Gordon, C., Kang, C. et al. (2013) Folate polyglutamylation eliminates dependence of activity on enzyme concentration in mitochondrial serine hydroxymethyltransferases from Arabidopsis thaliana. Archives of Biochemistry and Biophysics, 536, 87–96.
- Wingler, A., Lea, P.J. & Leegood, R.C. (1999) Photorespiratory metabolism of glyoxylate and formate in glycine-accumulating mutants of barley and *Amaranthus edulis. Planta*, 207, 518–526.
- Xie, Z., Yu, L., Yu, H. & Deng, Q. (2012) Application of a fluorescent derivatization reagent 9-chloromethyl anthracene on determination of carboxylic acids by HPLC. *Journal of Chromatographic Science*, 50, 464–468.
- Xu, Y., Fu, X., Sharkey, T.D., Shachar-Hill, Y. & Walker, B.J. (2021) The metabolic origins of non-photorespiratory CO₂ release during photosynthesis: a metabolic flux analysis. *Plant Physiology*, 186, 297–314.
- Zhang, Y., Sun, K. & Roje, S. (2008) An HPLC-based fluorometric assay for serine hydroxymethyltransferase. Analytical Biochemistry, 375, 367–369.
- Zhang, Y., Sun, K., Sandoval, F.J., Santiago, K. & Roje, S. (2010) One-carbon metabolism in plants: characterization of a plastid serine hydroxymethyltransferase. *Biochemical Journal*, **430**, 97–105.
- Zhang, Y., Zhang, C., Man, X., Men, Y., Ren, X., Li, X. et al. (2023) Functional characterization of the SiFPGS2 gene of foxtail millet in folate accumulation and root development. Plant Growth Regulation, 99, 137–147.
- Zimmermann, S.E., Benstein, R.M., Flores-Tornero, M., Blau, S., Anoman, A.D., Rosa-Téllez, S. et al. (2021) The phosphorylated pathway of serine biosynthesis links plant growth with nitrogen metabolism. Plant Physiology, 186, 1487–1506.